JAMES | Journal of Advances in Modeling Earth Systems

RESEARCH ARTICLE
10.1029/2025MS005270

Understanding the Drivers of Carbon–Nitrogen Cycle Variability in CMIP6 ESMs With MAGICC CNit v2.0: Model and Calibration Updates

Gang Tang[1,2], Sönke Zaehle[2], Zebedee Nicholls[3], Alexander Norton[4], Tilo Ziehn[4], and Malte Meinshausen[1]

[1]School of Geography, Earth and Atmospheric Sciences, The University of Melbourne, Melbourne, VIC, Australia, [2]Department of Biogeochemical Signals, Max Planck Institute for Biogeochemistry, Jena, Germany, [3]Energy, Climate and Environment (ECE) Program, International Institute for Applied Systems Analysis (IIASA), Laxenburg, Austria, [4]CSIRO Environment, Aspendale, VIC, Australia

Abstract Carbon–nitrogen coupling is a critical constraint for improving carbon cycle and climate simulations in Earth system models (ESMs), yet large uncertainties hinder inter-model comparisons. Here, we present CNit v2.0, an updated representation of the carbon–nitrogen cycle in MAGICC—a widely used reduced-complexity model (RCM). CNit v2.0 is calibrated to emulate carbon–nitrogen cycle dynamics in various ESMs across historical, idealized (1pctCO2, 1pctCO2-bgc), and multiple Shared Socioeconomic Pathway (SSP) experiments, demonstrating strong emulation performance. The global annual-mean emulation from historical to SSP5-8.5 (1850–2100) reveals increasing nitrogen limitation on net primary production (NPP), with a multi-model mean inhibition of 10.2 ± 5.6% by 2100 due to nitrogen deficits limiting plant uptake. The stronger CO_2 fertilization effect in carbon-only (C-only) ESMs exceeds the mitigating influence of nitrogen limitation in CN-coupled ESMs, implying a risk of continued NPP overestimation in C-only ESMs—even if a nitrogen cycle is later added—due to insufficient constraints on CO_2 sensitivity. The climate response of litter production is sign-changing between C-only (inhibition) and CN-coupled (enhancement) ESMs, suggesting nitrogen effects may be misattributed as climate effects in C-only ESMs. Divergent climate responses and nitrogen effects on litter decomposition—particularly litter respiration and labile soil organic matter decomposition—are the primary drivers of total heterotrophic respiration differences between C-only and CN-coupled ESMs. Alongside NPP, these factors shape distinct carbon cycle dynamics. While nitrogen pools and fluxes generally follow carbon trends, they exhibit greater inter-model spread. In light of the calibration updates, we propose practical strategies to improve carbon cycle calibration in future RCMs.

Plain Language Summary Carbon and nitrogen cycles interact closely to regulate Earth's climate and ecosystems. However, Earth system models (ESMs) differ in how they represent this coupling, complicating result comparisons. We developed CNit v2.0, an updated carbon–nitrogen cycle module within MAGICC, a widely used reduced-complexity model. CNit v2.0 is calibrated to emulate carbon–nitrogen cycle dynamics in 15 ESMs across historical, idealized, and scenario experiments, and it shows strong emulation performance. Our results reveal that nitrogen increasingly limits plant growth through the 21st century under high-emission scenarios, reducing global net primary production by about 10% by 2100. Models without a nitrogen cycle tend to overestimate plant growth due to stronger CO_2 fertilization effects (where higher CO_2 concentrations enhance growth). Nitrogen effects vary across turnover processes: they suppress litter production and decomposition while enhancing soil respiration. Moreover, the climate response of litter production differs in sign between models with and without nitrogen coupling. These patterns contribute to divergent carbon cycle responses across models. While nitrogen pools and fluxes generally follow carbon trends, they show greater inter-model variability. Based on these findings and prior calibrations, we propose practical strategies to improve carbon cycle calibration in future reduced-complexity models, enhancing the reliability of climate projections.

Key Points:

- CNit v2.0 explicitly simulates biological nitrogen fixation and plant nitrogen deficit, and applies more consistent calibrations
- CNit v2.0 effectively emulates carbon–nitrogen cycle behavior in 15 Earth system models across historical, idealized, and scenario runs
- Nitrogen deficit limits plant growth and litter production/decomposition but enhances soil respiration under high emission scenarios

Correspondence to:
G. Tang,
gang.tang.au@gmail.com;
gang.tang@student.unimelb.edu.au;
tgang@bgc-jena.mpg.de

Citation:
Tang, G., Zaehle, S., Nicholls, Z., Norton, A., Ziehn, T., & Meinshausen, M. (2026). Understanding the drivers of carbon–nitrogen cycle variability in CMIP6 ESMs with MAGICC CNit v2.0: Model and calibration updates. *Journal of Advances in Modeling Earth Systems*, *18*, e2025MS005270. https://doi.org/10.1029/2025MS005270

Received 2 JUN 2025
Accepted 3 DEC 2025

Author Contributions:

Conceptualization: Gang Tang, Malte Meinshausen
Data curation: Gang Tang
Formal analysis: Gang Tang
Funding acquisition: Gang Tang, Sönke Zaehle, Zebedee Nicholls, Alexander Norton, Tilo Ziehn, Malte Meinshausen
Investigation: Gang Tang
Methodology: Gang Tang, Sönke Zaehle
Software: Gang Tang, Zebedee Nicholls, Alexander Norton, Tilo Ziehn
Supervision: Sönke Zaehle, Zebedee Nicholls, Alexander Norton, Malte Meinshausen

1. Introduction

The inclusion of the nitrogen cycle represents a major advancement in Earth system models (ESMs) participating in the Coupled Model Intercomparison Project Phase 6 (CMIP6), compared to those from the CMIP5 era. The significance of this development has been emphasized in many studies (Hungate et al., 2003). For instance, the

Validation: Gang Tang
Visualization: Gang Tang
Writing – original draft: Gang Tang
Writing – review & editing: Sönke Zaehle, Zebedee Nicholls, Alexander Norton, Tilo Ziehn, Malte Meinshausen

implementation of an interactive carbon–nitrogen cycle helps address the overestimation of gross primary production (GPP, i.e., photosynthesis) seen in CMIP5 ESMs (Gier et al., 2024). Moreover, the absolute values of carbon–concentration and carbon–climate feedbacks are generally lower in carbon-nitrogen coupled (CN-coupled) ESMs than in carbon-only (C-only) ESMs (Arora et al., 2020). This nitrogen limitation effect on carbon cycle feedbacks can reduce their magnitude by up to 30% in individual ESMs (Ziehn et al., 2021). Including the nitrogen cycle also reduces uncertainties in the modeled historical land carbon sink and significantly affects future projections (Seiler et al., 2024; Zaehle et al., 2015).

These findings highlight the critical role of the nitrogen cycle in ESMs. However, incorporating nitrogen representations also introduces substantial uncertainties in the modeled nitrogen cycle and carbon–nitrogen coupling. An evaluation of the nitrogen cycle representation in land surface models participating in the TRENDY (Trends and Drivers of Terrestrial Sources and Sinks of Carbon Dioxide) project reveals large inter-model variability in the magnitudes and trends of multiple nitrogen-related variables (Kou-Giesbrecht et al., 2023). More importantly, such variability shows no correlation with carbon cycle variables or nitrogen process representations, suggesting a disconnect between the carbon and nitrogen cycles in these models. Divergent representations of key nitrogen cycle processes—such as biological nitrogen fixation (BNF) and ecosystem carbon:nitrogen stoichiometry—lead to varying estimates of BNF and other nitrogen fluxes and states, yet result in similar estimates of net primary production (NPP) or GPP (Davies-Barnard et al., 2022; Meyerholt et al., 2020). On one hand, these findings underscore the urgent need for observational constraints to improve nitrogen cycle modeling (Davies-Barnard et al., 2020; Zaehle et al., 2014). On the other hand, these findings draw attention to a critical question: What are the key differences driving the diverse carbon–nitrogen cycle behaviors in CMIP6 ESMs? A detailed comparison of the carbon–nitrogen cycle within a consistent framework is lacking, hindering efforts to attribute sources of variability and quantify associated uncertainties.

Due to the high computational demands of ESMs, running large ensembles for uncertainty analysis is impractical. Furthermore, implementing and testing diverse process formulations within a single ESM poses significant technical challenges. Therefore, emulation—using simplified, parameterized representations to mimic the dynamics of complex models—emerges as a practical alternative for exploring sources of variability and uncertainty (Wigley & Raper, 1987, 1992, 2001). MAGICC (Model for the Assessment of Greenhouse Gas Induced Climate Change) is one of the most widely used emulators, or reduced-complexity models (RCMs), in climate and carbon cycle studies (e.g., Climate Change 2014: Synthesis Report, IPCC, 2014; *Global Warming of* 1.5°C, IPCC, 2018; Climate Change 2023: Synthesis Report, IPCC, 2023). Its carbon–nitrogen module, CNit, is the first emulator to include a fully coupled carbon–nitrogen cycle (Tang, Nicholls, Norton, et al., 2025). From the CNit v1.0 calibration, we identified a consistent nitrogen limitation on NPP across many CMIP6 ESMs, persisting from 1850 to 2100 under a range of Shared Socioeconomic Pathway (SSP) scenarios. The calibration also revealed that, on average, nitrogen limitation suppresses litter production and decomposition, while enhancing soil respiration. However, limitations remain in our earlier emulation efforts, stemming from either parameterization choices or calibration setup (details discussed in Tang, Nicholls, Norton, et al. (2025)). As MAGICC provides the standard greenhouse gas concentration forcing for concentration-driven CMIP experiments, it is crucial to improve its model representation and calibration to better capture key carbon–nitrogen biogeochemical processes and feedbacks.

In this work, we present CNit v2.0, a revised and enhanced version of the original CNit model. We calibrate CNit v2.0 to 15 CMIP6 ESMs, including 10 CN-coupled and 5 C-only models, across historical, multiple SSPs, 1pctCO2, and 1pctCO2-bgc scenarios. Section 2 introduces the updates made in CNit v2.0 compared to v1.0. Section 3 describes the calibration procedures. In Section 4, we evaluate calibration performance by comparing ESM outputs with CNit simulations. With the calibrated parameters, we use emulation results from the historical and SSP5-8.5 scenario (collectively referred to as hist_ssp585) as a representative case to highlight key variabilities in carbon–nitrogen cycle fluxes and states in CMIP6 ESMs, and to identify the underlying drivers, which refer to the varying responses of different processes in the models. We present and discuss the results in Sections 5 and 6, respectively. In Section 7, we explore the implications of the updated calibration, from which we provide general recommendations for the carbon-nitrogen cycle calibration in RCMs. Finally, we summarize the model and calibration updates, highlight the key findings and their implications, and outline future applications of the calibrated CNit v2.0 in Section 8. The CNit v2.0 calibration demonstrates the model's ability to emulate the diverse carbon-nitrogen cycle behaviors in CMIP6 ESMs. Moving forward, we will apply the CNit v2.0, coupled with MAGICC's emission-driven online run framework, to generate probabilistic projections of climate and

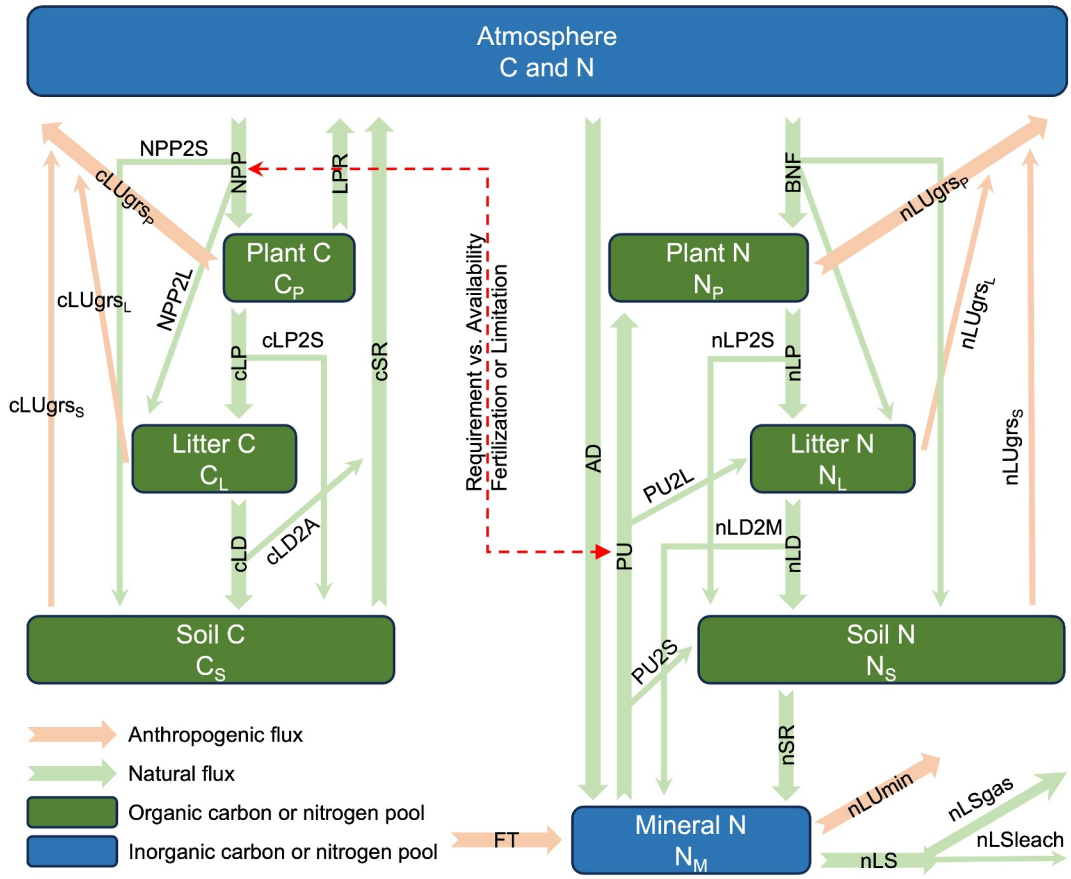

Figure 1. Schematic overview of the MAGICC CNit v2.0 model structure (NPP: net primary production; LPR: litter production respiration; PU: nitrogen plant uptake; BNF: biological nitrogen fixation; LP: litter production; LD: litter decomposition; SR: soil respiration; LS: mineral nitrogen loss; LU: land use emission; AD: atmosphere nitrogen deposition; FT: nitrogen fertilizer application; 2P, 2L, 2S, and 2M: the partition of fluxes into plant, litter, soil, and mineral pools). A complete list of flux and state variables in CNit v2.0, along with detailed descriptions, is provided in Table A1.

carbon cycle future, spanning a wide range of scenarios and highlighting the crucial role of nitrogen cycle feedbacks.

2. Model Description

2.1. Overview of the CNit v2.0

CNit v2.0 is a global box model comprising three carbon pools—plant (C_P), litter (C_L), and soil (C_S)—and four nitrogen pools—plant (N_P), litter (N_L), soil (N_S), and mineral (N_M). The model first computes key fluxes such as net primary production (NPP), litter production respiration (LPR), biological nitrogen fixation (BNF), and nitrogen plant uptake (PU). These modeled fluxes, along with input fluxes from nitrogen atmospheric deposition (AD), nitrogen fertilizer application (FT), and land use changes (LU, for both carbon and nitrogen), are used to solve a system of differential equations based on mass conservation. This yields the carbon and nitrogen states and turnover rates for each pool. The solved land carbon pool sizes determine the net land-to-atmosphere carbon flux, which is used to update the atmospheric CO_2 concentration and further inform the other modules (e.g., climate) in MAGICC (Meinshausen et al., 2011). The overall framework of CNit v2.0 (Figure 1) is similar to that of CNit v1.0 (Tang, Nicholls, Norton, et al., 2025), with updates to specific parameterizations and calculations. The design philosophy remains consistent with that of MAGICC: "be as simple as possible while as mechanistic as necessary in the sense of being based on physical principles and/or long-term ESM calibrations." In this section, we focus on the updates and highlight the key differences.

2.2. Carbon and Nitrogen Mass Conservation

Given the temporal resolution of interest in applications (e.g., annual), CNit partitions both NPP and cLUgrs (the carbon flux from land use perturbation due to gross deforestation) among the three carbon pools. The partitioning of NPP reflects turnover processes occurring within a single year. While NPP initially enters the plant pool, a substantial fraction is turned over within the same year (e.g., leaf and fine-root litter in deciduous forests) and thus does not persist in the annual-mean plant pool. To capture this, a fraction of NPP is directly allocated to the litter pool ($f_{\mathrm{NPP2L}} \times \mathrm{NPP}$) and to the soil pool ($f_{\mathrm{NPP2S}} \times \mathrm{NPP}$), in addition to the turnover fluxes explicitly represented in CNit. The partitioning of cLUgrs reflects that certain perturbations—such as biomass burning and land use conversion—can lead to emissions from the litter and soil pools within the same time step. Litter decomposition (cLD) is similarly partitioned, with a fraction transferred to the soil pool ($f_{\mathrm{cLD2S}} \times \mathrm{cLD}$) and the remainder released to the atmosphere as respiration ($f_{\mathrm{cLD2A}} \times \mathrm{cLD}$). The latter flux includes both direct litter respiration and the rapid mineralization of litter-derived, labile soil organic matter within the same year. The carbon mass balance equations for the plant, litter, and soil pools are as follows:

$$\frac{dC_P}{dt} = f_{\mathrm{NPP2P}} \times \mathrm{NPP} - \mathrm{LPR} - \mathrm{cLP} - f_{\mathrm{cLUgrs2P}} \times \mathrm{cLUgrs} \tag{1}$$

$$\frac{dC_L}{dt} = f_{\mathrm{NPP2L}} \times \mathrm{NPP} + f_{\mathrm{cLP2L}} \times \mathrm{cLP} - \mathrm{cLD} - f_{\mathrm{cLUgrs2L}} \times \mathrm{cLUgrs} \tag{2}$$

$$\frac{dC_S}{dt} = f_{\mathrm{NPP2S}} \times \mathrm{NPP} + f_{\mathrm{cLP2S}} \times \mathrm{cLP} + f_{\mathrm{cLD2S}} \times \mathrm{cLD} - \mathrm{cSR} - f_{\mathrm{cLUgrs2S}} \times \mathrm{cLUgrs} \tag{3}$$

The total heterotrophic respiration (RH) is:

$$\mathrm{RH} = \mathrm{LPR} + f_{\mathrm{cLD2A}} \times \mathrm{cLD} + \mathrm{cSR} \tag{4}$$

By summing the dynamics of the plant, litter, and soil carbon pools (Equations 1–4), the total change in land carbon pool size is obtained. Note that the sum of the partitioning fractions equals one, ensuring mass conservation:

$$\frac{dC_{\mathrm{Land}}}{dt} = \mathrm{NPP} - \mathrm{RH} - \mathrm{cLUgrs} \tag{5}$$

This change in the total land carbon pool also represents the net land carbon flux (cNetLand). It is conceptually similar to net biospheric production, with the key distinction that the latter includes carbon fluxes from product decay, which are not accounted for in cNetLand.

Consistent with the assumptions made for the carbon cycle, BNF, PU, and nLUgrs are partitioned among the three organic nitrogen pools. Similarly, nLD is partitioned between the soil and mineral nitrogen pools.

$$\frac{dN_P}{dt} = f_{\mathrm{BNF2P}} \times \mathrm{BNF} + f_{\mathrm{PU2P}} \times \mathrm{PU} - \mathrm{nLP} - f_{\mathrm{nLUgrs2P}} \times \mathrm{nLUgrs} \tag{6}$$

$$\frac{dN_L}{dt} = f_{\mathrm{BNF2L}} \times \mathrm{BNF} + f_{\mathrm{PU2L}} \times \mathrm{PU} + f_{\mathrm{nLP2L}} \times \mathrm{nLP} - \mathrm{nLD} - f_{\mathrm{nLUgrs2L}} \times \mathrm{nLUgrs} \tag{7}$$

$$\frac{dN_S}{dt} = f_{\mathrm{BNF2S}} \times \mathrm{BNF} + f_{\mathrm{PU2S}} \times \mathrm{PU} + f_{\mathrm{nLP2S}} \times \mathrm{nLP} + f_{\mathrm{nLD2S}} \times \mathrm{nLD} - \mathrm{nSR} - f_{\mathrm{nLUgrs2S}} \times \mathrm{nLUgrs} \tag{8}$$

The net mineralization (NetMIN)—a key flux supplying the mineral nitrogen pool—is defined as:

$$\mathrm{NetMIN} = f_{\mathrm{nLD2M}} \times \mathrm{nLD} + \mathrm{nSR} \tag{9}$$

Summing the dynamics of the plant, litter, and soil nitrogen pools (Equations 6–9) leads to the land organic nitrogen dynamics:

$$\frac{dN_{\text{Lando}}}{dt} = \text{BNF} + \text{PU} - \text{NetMIN} - \text{nLUgrs} \tag{10}$$

A new parameterized flux, nLUmin (nitrogen flux from land use perturbation in the form of mineral nitrogen loss), is introduced to model changes in the mineral nitrogen pool size. This flux distinguishes land use emissions from the organic pools (nLUgrs, e.g., deforestation and harvest) and the inorganic pool (nLUmin, e.g., fertilizer application and soil disturbance). Further details on the land use perturbation flux are provided in Section 2.3.

$$\frac{dN_M}{dt} = \text{AD} + \text{FT} + \text{NetMIN} - \text{PU} - \text{nLS} - \text{nLUmin} \tag{11}$$

The nLS represents the total nitrogen loss from the mineral pool, which includes both gaseous loss (nLSgas) and leaching (nLSleach). Summing the dynamics of the organic and mineral nitrogen pools (Equations 10 and 11) leads to the total land nitrogen conservation equation:

$$\frac{dN_{\text{Land}}}{dt} = \text{BNF} + \text{AD} + \text{FT} - \text{nLS} - \text{nLUgrs} - \text{nLUmin} \tag{12}$$

The resulting change in the land nitrogen pool also represents the net land nitrogen flux (nNetLand). As with previous versions of the carbon cycle in MAGICC (Meinshausen et al., 2011; Tang, Nicholls, Norton, et al., 2025), CNit v2.0 does not include a product pool for either carbon or nitrogen, due to its much smaller size relative to the other pools. Therefore, neither cNetLand nor nNetLand accounts for carbon or nitrogen fluxes from product decay.

2.3. Land Use Emission Calculation

In CNit v1.0, an updated implementation of land use emissions and their impact on NPP was introduced, based on the simple assumption of a constant regrowth rate during the regrowing period following any one-time deforestation (see Section 2.7 in Tang, Nicholls, Norton, et al. (2025)). By default, CNit v1.0 uses net land use emissions (for both carbon and nitrogen) as input, which is applicable in most model calibration and application scenarios. However, this is not always the case, such as when gross emissions are provided instead of net emissions in certain scenarios (e.g., CDR scenarios). In CNit v2.0, the same parameterizations are maintained, with the addition of a method option parameter (m_{cLU} and m_{nLU}) to accommodate flexible inputs. The following land use emission parameterizations apply to both carbon and nitrogen:

$$\text{LUnet}(t) = \text{LUgrs}(t) - \text{LUrgr}(t) \tag{13}$$

where LUnet, LUgrs, and LUrgr represent the carbon or nitrogen flux from land use perturbation in terms of net emission, gross deforestation, and regrowth, respectively. This relationship applies to the entire time series at each time step t.

For each instance of gross deforestation at time step t, a constant regrowth flux is applied during the regrowing period, starting at the subsequent time step ($t + 1$):

$$\text{LUrgr}(T) = \frac{\varphi \times \text{LUgrs}(t)}{\tau_{\text{rgr}}}, \forall\, T \in [t+1, t+\tau_{\text{rgr}}] \tag{14}$$

where φ is the regrowth fraction and τ_{rgr} is the regrowing time required to reach the partial regrowth. The total regrowth at time t is the sum of contributions from all gross emissions that occurred within the τ_{rgr} years preceding t, expressed as:

$$\text{LUrgr}(t) = \begin{cases} \sum_{T=\max(0,t-\tau_{rgr})}^{t-1} \frac{\varphi \times \text{LUgrs}(T)}{\tau_{\text{rgr}}} & \text{if } t \geq 1 \\ 0 & \text{if } t < 1 \end{cases} \tag{15}$$

Note that for $t < 1$, the initial year regrowth, LUrgr(0), is assumed to be zero, as regrowth by definition occurs only after gross deforestation. Since information prior to the start of the time series is unavailable for a given land use emission input, CNit v2.0 assumes that the gross deforestation and net emissions are equal in the initial year, that is, LUnet(0) = LUgrs(0) − 0.

The newly introduced method option parameters (m_{cLU} and m_{nLU}) function under the following conditions:

1. When LUnet is used as input (m_{cLU} or $m_{\mathrm{nLU}} = 0$, e.g., AFOLU (Agriculture, Forestry and Other Land Uses) carbon emissions), LUgrs and LUrgr are progressively solved at each time step to match the LUnet input time series.
2. When LUgrs is used as input (m_{cLU} or $m_{\mathrm{nLU}} = 1$, e.g., gross nitrogen emission), LUrgr time series is directly calculated (Equations 14 and 15), and LUnet is updated based on the calculated LUrgr.
3. When both LUgrs and LUrgr are provided as inputs (m_{cLU} or $m_{\mathrm{nLU}} = 2$), LUnet is simply calculated as the difference between the two (Equation 13).

For land use carbon, cLUrgr is further used in the NPP calculation (see Section 2.4). In addition to constructing the mass conservation of the carbon pools (Equations 1–5), cLUgrs is used to proxy the effect of land use on NPP (Tang, Nicholls, Norton, et al., 2025). For land use nitrogen, nLUgrs is used solely for mass conservation of the nitrogen pools (Equations 6–12). The nLUrgr and nLUnet are diagnostic fluxes and are not involved in the BNF or PU calculations, as these processes are proxied by NPP (see Section 2.6), which already accounts for the land use effect (see Section 2.4). The nLUmin represents gross emissions by definition, specifically the direct loss of mineral nitrogen from agricultural activities (e.g., AFOLU nitrogen emissions).

2.4. Refinements in NPP Formulation

NPP is one of the key fluxes modeled since the first MAGICC carbon cycle (Meinshausen et al., 2011). In CNit v1.0, we introduced the effect of carbon-nitrogen coupling and revised the impact of land use emissions (Tang, Nicholls, Norton, et al., 2025). In CNit v2.0, we further update the NPP formulation as follows:

$$\mathrm{NPP} = (\mathrm{NPP}_0 + \mathrm{cLUrgr}) \times \epsilon_{\mathrm{CO_2}} \times \epsilon_{dT(\mathrm{NPP})} \times \epsilon_{\mathrm{CN(NPP)}} \times \epsilon_{\mathrm{LU}} \tag{16}$$

The key change from CNit v1.0 is the addition of cLUrgr to NPP_0 (the baseline NPP). Both terms are then influenced by CO_2 fertilization ($\epsilon_{\mathrm{CO_2}}$), temperature effects ($\epsilon_{dT(\mathrm{NPP})}$), carbon-nitrogen coupling effects ($\epsilon_{\mathrm{CN(NPP)}}$), and land use effects (ϵ_{LU}). The parameterizations for these effects remain unchanged from CNit v1.0.

In CNit v1.0, cLUnet was directly used in the mass conservation calculation (where cLUnet = cLUgrs − cLUrgr, maintaining mass conservation) (Tang, Nicholls, Norton, et al., 2025). This approach effectively treated regrowth as an additional flux, independent of environmental factors, providing a simpler calculation but sacrificing its mechanistic interpretation. The updated formulation in CNit v2.0 treats cLUrgr as the baseline regrowth after deforestation, which is then scaled by the effects of CO_2, temperature, nutrients, and additional land use perturbations. This update improves the representation of the ecological behavior of regrowth.

2.5. Explicit Representation of Nitrogen Deficit and Its Effect on NPP

In CNit v1.0, the nitrogen deficit was implicitly calculated from the nitrogen requirement for PU (PUreq) and AD, based on the approximation that NetMIN is linearly correlated with PU (see details in Tang, Nicholls, Norton, et al. (2025)). In the updated version, we first calculate the potential NPP (NPPpot) using Equation 16, by setting $\epsilon_{\mathrm{CN(NPP)}} = 1$ (i.e., no nitrogen effect). PUreq is determined by NPPpot and a nitrogen-to-carbon ratio, reflecting the requirement for plants to maintain a specific carbon-to-nitrogen stoichiometry during carbon assimilation:

$$\mathrm{PUreq} = \mathrm{NPPpot} \times \mathrm{nc}_{\mathrm{NPPpot}} \tag{17}$$

Next, we calculate the nitrogen availability for PU (PUavail) from two sources: the current AD (assuming all deposition is immediately available for plant uptake) and the NetMIN available for plant uptake ($\mathrm{PUavail}_{\mathrm{NetMIN}}$). For $\mathrm{PUavail}_{\mathrm{NetMIN}}$, we further separate it into two components: one is the portion of the current NetMIN available for plant uptake, and the other is long-term NetMIN, which accumulates in the mineral nitrogen pool and becomes available for plant uptake at the current time step. The former is modeled by a baseline NetMIN (NetMIN_0),

which includes a temperature effect scalar—expressed in exponential form with sensitivity parameter sNetMIN2dT—as NetMIN (decomposition) rates are temperature-dependent. The latter is parameterized as a baseline long-term NetMIN (NetMIMlt$_0$), scaled by the NPPpot/NPP$_0$ ratio and an exponential response to AD, with sensitivity sNetMINlt2AD. The NPPpot/NPP$_0$ considers that NPP determines the quantity of newly formed organic carbon (i.e., the substrate for decomposition/mineralization, Equation 9), thereby controlling the baseline rate for long-term NetMIN. The effect of AD incorporates the understanding that NetMIN is a nitrogen-demanding process (NetMIN = mineralization—immobilization) (Cheng et al., 2019). Collectively, the PUavail is derived from:

$$\mathrm{PUavail} = \mathrm{AD} + \mathrm{NetMIN}_0 \times e^{s_{\mathrm{NetMIN2dT}} \times dT} + \mathrm{NetMINlt}_0 \times \frac{\mathrm{NPP}_{\mathrm{pot}}}{\mathrm{NPP}_0} \times e^{s_{\mathrm{NetMINlt2AD}} \times \mathrm{AD}} \tag{18}$$

The parameterization of PUavail effectively approximates mineral nitrogen availability for plant uptake without explicitly relying on the current mineral nitrogen pool size. This approximation is necessary due to the emulator's annual time scale, where the mineral nitrogen pool is substantially smaller than the total annual mineral nitrogen demand.

With both the PUreq and PUavail, the nitrogen deficit relative to PU demand (PUdef) is determined as:

$$\mathrm{PUdef} = \mathrm{PUreq} - \mathrm{PUavail} \tag{19}$$

The effect of nitrogen deficit on NPP is given by:

$$\epsilon_{\mathrm{CN(NPP)}} = e^{s_{\mathrm{NPP2PUdef}} \times \mathrm{PUdef}} \tag{20}$$

where $s_{\mathrm{NPP2PUdef}}$ represents the sensitivity of NPP to PUdef. The resulting $\epsilon_{\mathrm{CN(NPP)}}$ is then used in Equation 16 to calculate the actual NPP (NPPact). NPPact is incorporated into the mass conservation equations (Equations 1–5) to determine the carbon pool size dynamics.

2.6. PU and BNF Simulation

In CNit v1.0, the simulation of actual PU (PUact) is based on NPPact and a temperature response. This approach is effective for most ESMs, where a near-linear correlation between NPP and PU is commonly observed (Tang, Nicholls, Norton, et al., 2025). However, in certain cases, such as MIROC-ES2L and UKESM1-0-LL, this relationship is less evident in their 1pctCO2 simulations, suggesting a weak coupling between NPP and PU under that experimental design. As an emulator, CNit seeks to capture the best representation across all experiments, which can sometimes lead to simultaneous overestimation of PU and underestimation of NPP (or vice versa) when the assumed relationship does not hold (e.g., for the 1pctCO2 runs from MIROC-ES2L and UKESM1-0-LL). To enhance the emulation capacity and flexibility of CNit, the updated PUact parameterization replaces the previous exponential formulation (with a −1/NPPact exponent) with a sigmoidal response to NPPact, and introduces an additional exponential downregulation by PUdef. The temperature response remains unchanged, retaining its exponential form.

$$\mathrm{PUact} = \mathrm{PU}_0 \times \frac{\epsilon_{\mathrm{NPP(PU)max}}}{1 + (\epsilon_{\mathrm{NPP(PU)max}} - 1) \times e^{-s_{\mathrm{PU2NPP}} \times \left(\frac{\mathrm{NPPact}}{\mathrm{NPP}_0} - 1\right)}} \times e^{s_{\mathrm{PU2PUdef}} \times \mathrm{PUdef}} \times e^{s_{\mathrm{PU2dT}} \times dT} \tag{21}$$

where PU$_0$ is the baseline PU; $\epsilon_{\mathrm{NPP(PU)max}}$ defines the maximum scaling effect of NPP on PU; s_{PU2NPP} represents the sensitivity of PU to relative changes in NPP; s_{PU2PUdef} denotes the sensitivity of PU to the PUdef; and s_{PU2dT} is the sensitivity of PU to the temperature change.

This formulation reflects the concept that PUact is primarily driven by NPPact, with an upper limit defined by $\epsilon_{\mathrm{NPP(PU)max}}$. The effect of PUdef accounts for the direct regulation of nitrogen uptake by the balance between nitrogen availability and plant demand. The temperature effect captures the temperature sensitivity of enzymatic activity and root metabolism associated with the nitrogen uptake process.

In CNit v1.0, BNF is prescribed. In the updated version, a formulation analogous to the PU simulation is adopted for BNF, reflecting their shared role in supporting plant nitrogen demand for carbon assimilation (McNeill & Unkovich, 2007). However, different baseline rate (BNF_0), response to NPPact ($\epsilon_{NPP(BNF)max}$ and $s_{BNF2NPP}$), sensitivity to PUdef ($s_{BNF2PUdef}$), and temperature sensitivity (s_{BNF2dT}) are applied, reflecting both the distinct nature of the two processes and the diversity in how this process is represented across current ESMs (Davies-Barnard et al., 2022).

$$BNF = BNF_0 \times \frac{\epsilon_{NPP(BNF)max}}{1 + (\epsilon_{NPP(BNF)max} - 1) \times e^{-s_{BNF2NPP} \times \left(\frac{NPPact}{NPP_0} - 1\right)}} \times e^{s_{BNF2PUdef} \times PUdef} \times e^{s_{BNF2dT} \times dT} \tag{22}$$

2.7. Revision of the Carbon-Nitrogen Coupling Effect on Turnovers

In CNit v1.0, organic carbon and nitrogen turnovers follow a first-order decay process within the box model, with turnover fluxes calculated as the pool size divided by a turnover time (τ) and scaled by the carbon-nitrogen coupling effect (ϵ_{CN}) and the temperature effect (ϵ_{dT}).

$$turnover = \frac{poolsize_i}{\tau_i} \times \epsilon_{CN} \times \epsilon_{dT} \tag{23}$$

where i refers to the plant, litter, and soil carbon/nitrogen pools, excluding the mineral nitrogen pool. The proxies for the carbon-nitrogen coupling effect in all carbon and nitrogen turnovers, with the exception of mineral nitrogen turnover, are PUact and AD (Tang, Nicholls, Norton, et al., 2025).

In this update, we replace PUact with PUdef, which more accurately reflects the nitrogen status of the plant, as PUact does not provide information on whether the plant is nitrogen-limited. Additionally, the effect of AD is removed from the carbon-nitrogen coupling in the turnover processes, as it should be considered a secondary effect. Specifically, AD must first enrich the mineral nitrogen, which is then taken up by the plant before it can influence turnover rates. Since AD is already accounted for in the nitrogen deficit calculation (Equations 18 and 19), where PUdef serves as the proxy for the carbon-nitrogen coupling effect, removing AD prevents double counting of the mineral nitrogen enrichment effect. The new, simplified formulation for the ϵ_{CN} is as follows:

$$\epsilon_{CN(i)} = e^{s_{i2PUdef} \times PUdef} \tag{24}$$

where $s_{i2PUdef}$ refer to the sensitivity of turnover process i to PUdef.

The temperature effect retains the same exponential form:

$$\epsilon_{dT(i)} = e^{s_{i2dT} \times dT} \tag{25}$$

where s_{i2dT} represents the temperature sensitivity of turnover process i.

For the mineral nitrogen turnover, nLS, it is calculated as:

$$nLS = \frac{N_M}{\tau_{N_M}} \times \left[f_{nLS2A} \times \epsilon_{dT(nLSgas)} + \left(1 - f_{LS2A}\right)\right] \tag{26}$$

where N_M is the mineral nitrogen pool size, τ_{N_M} is the turnover time of the mineral nitrogen pool, and f_{nLS2A} is the fraction of nLS released to the atmosphere. The first component of nLS, representing gaseous loss (nLSgas), is assumed to be temperature-sensitive (Maag & Vinther, 1996) and is therefore scaled by its temperature response $\epsilon_{dT(nLSgas)}$, which is calculated by:

$$\epsilon_{dT(nLSgas)} = e^{s_{nLSgas2dT} \times dT} \tag{27}$$

The second component, nitrogen leaching (nLSleach), is assumed to be directly proportional to the size of the mineral nitrogen pool.

Table 1
Details of the Calibrated CMIP6 ESMs and Availability of Additional Experiment Data

Model	Land component	Variant label	SSP1-1.9	SSP4-6.0	1pctCO2-bgc	Reference
ACCESS-ESM1-5	CASA-CNP, CABLE2.4	r1i1p1f1	No	No	Yes	Ziehn et al. (2020)
CMCC-CM2-SR5	CLM4.5	r1i1p1f1	No	No	No, use it from CMCC-ESM2	Lovato et al. (2022)
CMCC-ESM2	CLM4.5, BGC configuration	r1i1p1f1	No	No	Yes	Lovato et al. (2022)
MIROC-ES2L	MATSIRO6.0, VISIT-e v1.0	r1i1p1f2	Yes	No	Yes	Hajima et al. (2020)
MPI-ESM1-2-LR	JSBACH3.2	r1i1p1f1	Yes	No	Yes	Mauritsen et al. (2019)
NorESM2-LM	CLM5	r1i1p1f1	No	No	Yes	Seland et al. (2020)
NorESM2-MM	CLM5	r1i1p1f1	No	No	No, use it from NorESM2-LM	Seland et al. (2020)
UKESM1-0-LL	JULES-ES-1.0	r1i1p1f2	Yes	No	Yes	Sellar et al. (2020)
CESM2-WACCM	CLM5	r1i1p1f1	No	No	No, use it from CESM2	Danabasoglu et al. (2020)
TaiESM1	CLM4	r1i1p1f1	No	No	No, leave it empty	Wang et al. (2021)
BCC-CSM2-MR	BCC-AVIM2	r1i1p1f1	No	No	Yes	Wu et al. (2021)
CNRM-ESM2-1	ISBA-CTRIP, ISBA-CC, SURFEX v8.0	r1i1p1f2	Yes	Yes	Yes	Séférian et al. (2019)
CanESM5	CLASS3.6, CTEM1.2	r1i1p1f1	Yes	Yes	Yes	Sigmond et al. (2023)
CanESM5-1	CLASS3.6, CTEM1.2	r1i1p1f1	Yes	Yes	No, use it from CanESM5	Sigmond et al. (2023)
IPSL-CM6A-LR	ORCHIDEE v2.0, Water/Carbon/Energy mode	r1i1p1f1	Yes	Yes	Yes	Boucher et al. (2020)

Note. Experiment data for historical, SSP1-2.6, SSP2-4.5, SSP3-7.0, SSP5-8.5, and 1pctCO2 experiments are available for all ESMs and are therefore not shown.

3. Model Calibration

3.1. Target Variables, Experiments, and CMIP6 ESMs

In this study, we focus on calibrating CNit v2.0 to the CMIP6 ESMs. The target variables for calibration include key carbon and nitrogen fluxes (NPP, RH, PU, BNF, NetMIN), as well as all the carbon and nitrogen pool sizes (C_P, C_L, C_S, N_P, N_L, N_S, and N_M). The corresponding variable names in the CMIP6 published data are listed in Table A1.

The target experiments consist of the historical runs, the four Tier-1 SSP scenarios in ScenarioMIP (SSP1-2.6, SSP2-4.5, SSP3-7.0, and SSP5-8.5) (O'neill et al., 2016), and two idealized scenarios (1pctCO2 and 1pctCO2-bgc). Additionally, the SSP1-1.9 and SSP4-6.0 experiments are included in the calibration where data is available (Table 1). For clarity, we refer to the combined historical and SSP scenarios as the hist_ssp experiments in this paper. The 1pctCO2 experiment is an idealized scenario in which atmospheric CO_2 concentration increases by 1% per year until it quadruples (~140 years) from its preindustrial value (284.317 ppm in 1850). Concentrations of other greenhouse gases and land use are held constant at preindustrial levels, making this experiment useful for diagnosing carbon cycle feedbacks in ESMs. The 1pctCO2-bgc experiment is based on 1pctCO2 but with the CO_2 increase masked from the climate module (i.e., the rise in CO_2 does not induce warming), thereby isolating the "pure" CO_2 effect on biogeochemical cycles. The inclusion of the 1pctCO2 and 1pctCO2-bgc scenarios provides effective calibration constraints, allowing for the separation of the CO_2 fertilization effect and the temperature effect on NPP, as well as the climate response and the carbon-nitrogen coupling effect on pool turnovers.

Based on data availability from the Earth System Grid Federation (ESGF, https://esgf-node.llnl.gov/projects/cmip6/, last accessed: 9 April, 2025), a total of 15 ESMs (10 CN-coupled and 5 C-only, Table 1) are included in the calibration, covering all 11 ESMs from the CMIP6 carbon cycle feedback evaluation study (Arora et al., 2020). CNit is technically composed of a carbon cycle module and a nitrogen cycle module (Figure 1). The model design enables the emulation of C-only ESMs by activating only the carbon cycle component and disabling the nitrogen cycle and carbon-nitrogen coupling (i.e., calibrating only the carbon-related parameters in CNit v2.0 to carbon fluxes and pool sizes for C-only ESMs). This design aligns with the goal of CNit, which is to evaluate and compare C-only and CN-coupled ESMs within a consistent framework, thereby synthesizing a comprehensive picture of current model-based understanding of the biogeochemical cycle.

For ESMs that submitted ensemble run results (e.g., from different realizations, initializations, model physics, and forcings, as indicated by the variant label in the CMIP6 global attributes), we calibrate only the ensemble member with the most complete data, typically the one labeled as "r1i1p1f1" (Table 1). It is important to note that output from the 1pctCO2-bgc scenario is not available for all selected ESMs. In such cases, we use data from a similar ESM (if available) as a substitute. For example, CMCC-CM2-SR5 does not provide results for the 1pctCO2-bgc scenario, whereas CMCC-ESM2 does. Since both ESMs share identical land components and exhibit very similar behavior in the historical and SSP experiments, we use the 1pctCO2-bgc results from CMCC-ESM2 as the target when calibrating CMCC-CM2-SR5. Details about the ESMs and data availability are provided in Table 1.

3.2. Data Collection and Post-Processing

In addition to the target variables (Table A1), we also obtained model-specific grid area data (areacella) and land fraction data (sftlf) to convert the monthly gridded data into global annual-mean values, as both CNit and MAGICC run on an annual time step by default.

During our previous analysis of the CMIP6 ESM outputs, we identified a mass conservation issue from the published data—specifically, a significant mismatch between the flux and pool size data (Tang, Nicholls, Jones, et al., 2025). The primary causes of this issue include incomplete data publication (e.g., some ESMs did not provide land use emission data) and inconsistencies in model definitions across different model intercomparison projects (e.g., land use emissions in C4MIP and LUMIP). This mass conservation issue poses challenges to our calibration, as both fluxes and pool sizes are part of the calibration targets. To harmonize the target variables and address this issue, we implemented the following workaround for the original outputs in the current calibration:

1. For carbon, we used the AFOLU carbon emission (Emissions|CO2|MAGICC AFOLU) from the Reduced Complexity Model Intercomparison Project (RCMIP) data set (Nicholls et al., 2021) as the cLUnet input for CNit v2.0 (Equations 13–15). Historical emissions are based on a combination of PRIMAP-hist Version 1.0 (1850–1959, PRIMAP—Potsdam Realtime Integrated Model for probabilistic Assessment of emissions Paths) (Gütschow et al., 2016) and the Global Carbon Budget 2016 (1959–2014) (Le Quéré et al., 2016). Future emissions from 2015 to 2100 are taken from the Intergovernmental Panel on Climate Change (IPCC)'s Sixth Assessment Report (AR6) Scenario Database (Byers et al., 2022; Gidden et al., 2019). By using the AFOLU emission, the gross land use emission modeled in CNit will unavoidably differ from the original ESM outputs. However, this approach represents the minimal modification necessary to maintain mass conservation. Without this method, we would have to revise the state variables in the ESM outputs or introduce additional carbon fluxes to account for the mass imbalance (with cumulative imbalance to hundreds of gigatons of carbon, (Tang, Nicholls, Jones, et al., 2025)). Such an approach would be undesirable and difficult to justify. The use of AFOLU emissions as input provides a clear method to account for land use emissions. Additionally, as part of the AR6 scenario database, incorporating the AFOLU emissions ensures consistency between the calibration and future applications of the MAGICC model in scenario simulations.
2. Similarly, we used the AFOLU nitrogen emissions (the sum of Emissions|N2O|MAGICC AFOLU, Emissions|NH3|MAGICC AFOLU, and Emissions|NOx|MAGICC AFOLU) (Byers et al., 2022; Nicholls et al., 2021) as the nLUmin input for CNit, and set the nLUgrs to zero. This treatment assumes that all nitrogen gross emissions are directly removed from the mineral nitrogen pool. This assumption is based on the fact that the dominant nitrogen emission species, NH3, primarily arises from agricultural activities that directly perturb the mineral nitrogen pool.
3. It is important to note that applying steps 1 and 2 provides a consistent and reasonable approach to handling the land use emission input but does not fully resolve the mass conservation issue in the data. While the value of the mass imbalance should change, it remains after applying the AFOLU emission input. To reconcile the flux and pool size, we employed a method similar to that used in our CNit v1.0 calibration (Tang, Nicholls, Norton, et al., 2025), which was also suggested in our CMIP6 data conservation analysis (Tang, Nicholls, Jones, et al., 2025). First, we retained the pool size data, as well as NPP, PU, and BNF, in accordance with the ESM outputs (i.e., we assume the state variables and major fluxes are more reliable). Then, we reconstructed the RH and NetMIN using mass conservation equations (Equations 1–12) and used them as the calibration targets. This approach prioritizes the calibration of state variables while addressing the imbalance in fluxes—whether from land use change, fire, or other processes—by incorporating them into RH and NetMIN. From a mass conservation perspective, this is reasonable because we do not alter the destination of these fluxes. Although we considered introducing the imbalance flux as a separate prescribed flux, such an approach would be model-

specific and experiment-specific, making it difficult to implement in future model applications. As a result, we chose not to pursue this approach.

4. CNit v2.0 requires nitrogen inputs for atmospheric deposition and fertilizer application (AD and FT in Equations 11 and 12). For AD, we used nitrogen deposition data from the CMIP6 forcing data sets (input4MIPs, the sum of dry and wet deposition for both NHx and NOy, (Hegglin et al., 2016)) rather than the ESM outputs (fNdep). This decision was based on two considerations: first, fNdep is not always available from ESM outputs; second, in many cases, the calculated global annual-mean fNdep does not align with the nitrogen deposition values in input4mips, although the magnitudes and trends are similar. This discrepancy indicates that while ESMs likely use the nitrogen deposition in input4MIPs as the nitrogen forcing, there may be some numerical differences when reconstructing the global value. Since the goal of this calibration, and subsequent applications, is to examine the responses of different processes rather than explore discrepancies caused by the input data, we used the input4MIPs nitrogen deposition consistently for all the ESM calibrations. Similarly, we used fertilizer application data from the input4MIPs (Land-Use Harmonization (LUH2), the management data (Hurtt et al., 2020)) for all calibrations.
5. Due to the limited availability of nitrogen loss flux data in ESM outputs (fNloss, fN2O, and fNleach), combined with the aforementioned mass conservation issues, and our decision to use AFOLU nitrogen emissions, input4MIPs nitrogen deposition, and LUH2 fertilizer application as inputs (nLUmin, AD, and FT), we did not use the ESM nitrogen loss outputs as calibration targets. Instead, we set the mineral nitrogen pool size as the target to allow CNit v2.0 to capture the dynamics of mineral nitrogen. This approach is reasonable because when we set influxes and pool sizes as targets, the total ecosystem outflux will be automatically constrained. While we have updated our parameterization for the nitrogen loss term (Equation 26), we do not fully utilize its capacity due to the lack of data for separating gaseous loss and leaching loss. Therefore, we fixed the gaseous loss fraction, f_{nLS2A}, to 1 in the current calibration, assuming that all nitrogen losses occur as gaseous emissions and are influenced by temperature.

3.3. Calibration Process

The inputs for CNit v2.0 include cLUnet (and/or cLUgrs), nLUnet (and/or nLUgrs), nLUmin, AD, and FT (Figure 1). As detailed in the previous section, we used AFOLU emissions for cLUnet and nLUmin, and input4MIPs data for AD and FT, to ensure consistent inputs across all ESMs used in the calibration (Figure A1).

For the target variables, each SSP scenario was combined with the corresponding historical experiment to form a continuous hist_ssp time series from 1850 to 2100. For the 1pctCO2 and 1pctCO2-bgc experiments, we used the first 150 years of data, which is the common length provided by most ESMs, even though some ESMs extend to 165 years.

This offline calibration was conducted using output from the concentration-driven ESM simulations. The calibration procedure followed that described in the CNit v1.0 calibration study (Tang, Nicholls, Norton, et al., 2025). Briefly, we prescribed the land surface global-mean temperature (derived from the ESM output variable tas) and atmospheric CO_2 concentration (from input4MIPs (Meinshausen et al., 2017, 2020)) to drive CNit. The prescribed temperature and CO_2 trajectories are shown in Figure A1.

The cost function for the calibration was defined as the sum of normalized squared errors across the selected fluxes and pool sizes. For each target variable, the normalized error was calculated as:

$$\mathrm{cost}(\mathrm{var}) = \left(\frac{\mathrm{emulation} - \mathrm{target}}{\mathrm{target} \times \frac{\mathrm{target}_{\max} - \mathrm{target}_{\min}}{\overline{\mathrm{target}}}} \right)^2 \tag{28}$$

This formulation scales the squared error between the model emulation and the ESM target by the product of the target itself and a dimensionless factor that captures the temporal range of the target time series normalized by its mean. The purpose of this normalization is twofold: first, it ensures that variables with larger magnitudes or greater variability do not dominate the cost function; second, it allows for more balanced weighting across variables with different units or orders of magnitude. This approach facilitates a fair comparison and integration of diverse target variables in the overall cost function.

All experiments for each ESM were calibrated simultaneously, with the total cost function computed as the sum of unweighted errors across all experiments, resulting in a single set of parameters for each ESM. Using one parameter set to emulate an ESM across multiple experiments aligns with CNit's goal as a universal framework capable of reproducing ESM behavior under varying forcings (since ESMs run different experiments with different input forcing rather than different parameter values). Although this approach may reduce emulation performance—because the simplified framework may not fully capture non-linear responses across experiments—it remains the preferred strategy for emulators. Calibrating parameters separately for each experiment would also limit CNit's reliability in projecting broader scenarios, particularly when the calibration experiment differs substantially from the target scenarios.

The calibration followed a two-step procedure. First, global optimization was performed using the Differential Evolution algorithm (Storn & Price, 1997), with 30,000 iterations and five random initializations. The resulting five parameter sets were then used as initial values for the Nelder–Mead algorithm (Gao & Han, 2012), which was applied for local minimization with a maximum of 2,000 iterations per initialization. The parameter set yielding the lowest total cost was selected as the final calibrated result. A complete list of the calibrated parameter values for the 15 ESMs is archived on Zenodo (Tang, Zaehle, et al., 2025).

4. Evaluation of Emulation Performance Against ESM Outputs

The calibrated CNit v2.0 model effectively emulates the carbon-nitrogen cycle in the studied CMIP6 ESMs, as evidenced by its reproduction of key fluxes and pool sizes (Figure 2), although performance varies across variables, experiments, and models. The error for the emulated NPP fluctuates around zero in most cases. The mean error for NPP remains within ±1.0 GtC/yr for all ESMs across all experiments, with the majority falling within ±0.4 GtC/yr. Exceptions include the 1pctCO2 experiment, where the CNit emulation underestimates NPP for MPI-ESM1-2-LR and overestimates it for CanESM5-1 (mean errors across 1pctCO2 experimental period of approximately −3.5 GtC/yr and +1.2 GtC/yr, respectively).

The emulation error for C_{Land} is within ±20.0 GtC for most ESMs across their hist_ssp runs, with a mean error within ±5.0 GtC (relative error <0.5%). Larger errors are observed for UKESM1-0-LL and BCC-CSM2-MR, where the mean error ranges from approximately −7.0 to −20.0 GtC, corresponding to a ∼0.6%–∼1.0% underestimation. In the hist_ssp370 and hist_ssp585 scenarios, the two CanESM models exhibit larger emulation errors, with mean values of approximately −10.0 GtC and −20.0 GtC (relative errors of ∼0.4% and ∼0.7%), respectively. In the 1pctCO2 and 1pctCO2-bgc scenarios, maximum emulation errors range from 30.0 to 80.0 GtC for most ESMs, with both positive and negative biases. Exceptions with lower emulation errors (<20.0 GtC) include the two CMCC models (in both scenarios), TaiESM1 (in 1pctCO2), and CNRM-ESM2-1 (in 1pctCO2-bgc). Larger emulation errors are observed for the two CanESM models and BCC-CSM2-MR. Specifically, the emulation systematically underestimates C_{Land} in the two CanESM models, with mean errors of approximately −220.0 GtC in the 1pctCO2 scenario and −150.0 GtC in the 1pctCO2-bgc scenario (relative errors of ∼8.0% and ∼5.0%, respectively). Conversely, it overestimates C_{Land} for BCC-CSM2-MR, with mean errors of approximately +100.0 GtC in the 1pctCO2 scenario and +75.0 GtC in the 1pctCO2-bgc scenario (relative errors of ∼4.0% and ∼2.5%, respectively). The soil carbon pool contributes significantly to these emulation errors (not shown). These results indicate that the carbon cycle behaves differently in the hist_ssp and idealized scenarios within the ESMs, in ways that are not well represented by the CNit model. Nevertheless, these errors are still smaller than the intermodal differences in land carbon sequestration (with a standard deviation of 356.4 GtC over the whole experimental period) observed among the studied CMIP6 ESMs in the 1pctCO2 scenario.

For the cNetLand flux, emulation errors generally fluctuate around zero, with most errors falling within ±1.0 GtC/yr. The mean error for cNetLand is less than 0.2 GtC/yr for most ESMs in most of the experiments. Higher emulation errors are observed for BCC-CSM2-MR and the two CanESM models, with mean errors reaching approximately 0.6 GtC/yr and −0.8 GtC/yr, respectively, in the hist_ssp runs, and 2.0 GtC/yr and −4.0 GtC/yr in their 1pctCO2 runs.

The above results demonstrate that the CNit emulation captures both the fluxes and states in the land carbon cycle from CMIP6 ESMs, especially in the hist_ssp experiments. The more pronounced emulation errors for C_{Land} and cNetLand in the 1pctCO2 scenario can be attributed to multiple factors. First, the AFOLU land use emissions input used in CNit differs from the original ESM outputs (as explained in Section 3.2). Although we acknowledge this difference, it was the best available option for ensuring consistency. Second, CNit does not simulate fire

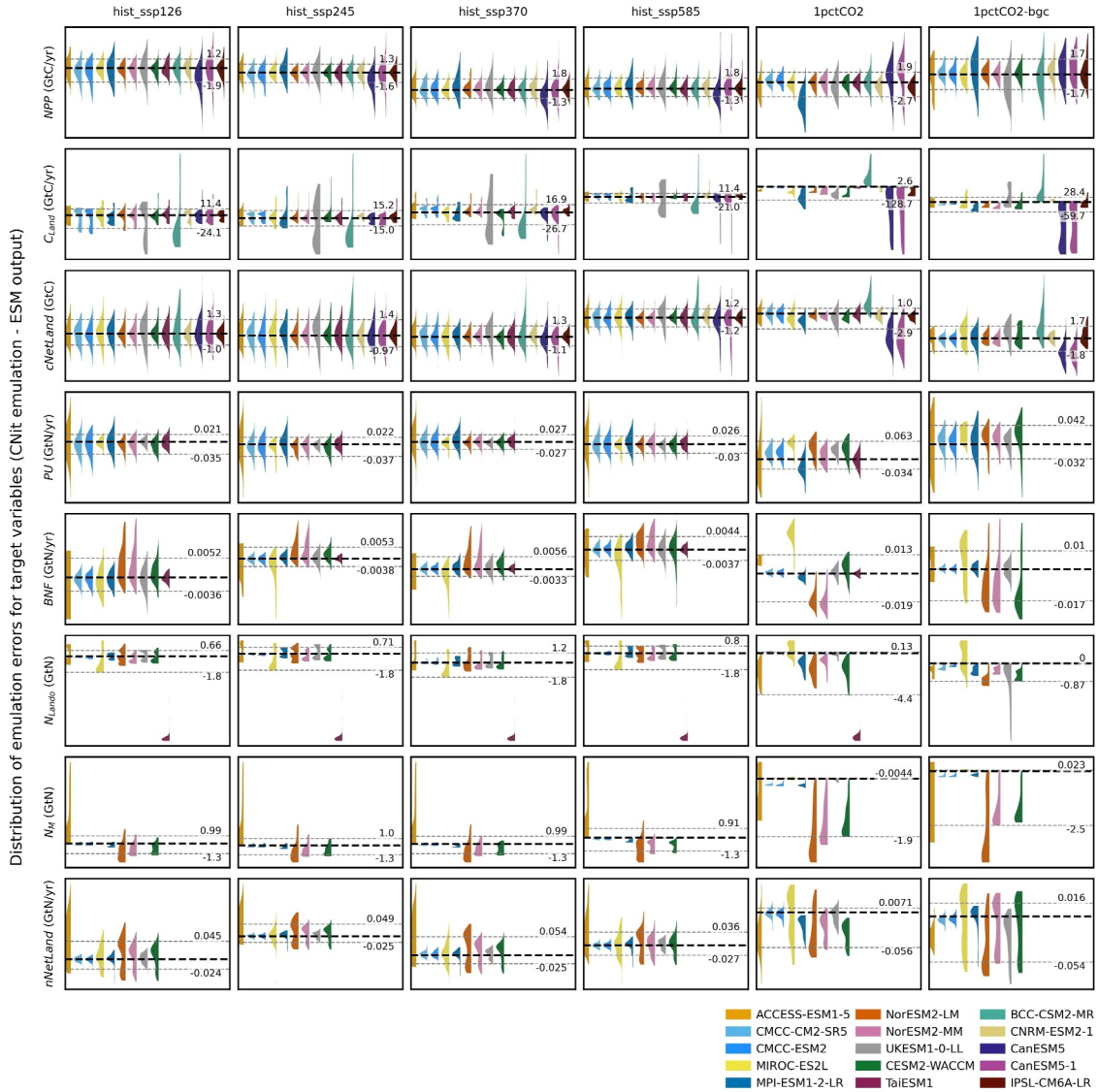

Figure 2. Distribution of emulation errors for target variables, including net primary production (NPP), land carbon pool size (C_{Land}), net land carbon flux (cNetLand), nitrogen plant uptake (PU), biological nitrogen fixation (BNF), land organic nitrogen pool size (N_{Lando}), mineral nitrogen pool size (N_M), and net land nitrogen flux (nNetLand), across the hist_ssp series, 1pctCO2, and 1pctCO2-bgc experiments. Gray dashed lines (with annotations) indicate the 10th to 90th percentile range of emulation errors across all CMIP6 ESMs within each experiment. Black dashed lines (unlabeled) indicate zero error.

emissions, while most of the selected CMIP6 ESMs do (Rabin et al., 2017). As a result, fire emissions are embedded within heterotrophic respiration (i.e., pool turnover) simulated by CNit (see Section 3.2). Since fire emissions differ significantly between the hist_ssp and 1pctCO2 experiments, calibrating these experiments together in CNit results in the use of identical turnover parameters (e.g., turnover time and sensitivity) to model fluxes that are not only largely different but also not inherently part of the turnover flux itself. Therefore, the emulation performance decreases. Third, other ESM components that drive the carbon cycle, such as precipitation and the water cycle, may respond differently to the hist_ssp and 1pctCO2 forcings. CNit does not account for these differences, which affects its ability to capture the distinct carbon cycle behaviors between the hist_ssp and idealized scenarios. Lastly, we calibrate all experiments simultaneously. As a result, the hist_ssp experiments carry more weight than the 1pctCO2 and 1pctCO2-bgc experiments, leading the calibration to favor the hist_ssp scenarios when they diverge from the idealized scenarios, in order to minimize the global cost function.

The emulated PU and BNF closely match the CMIP6 ESM outputs, with absolute errors <0.2 GtN/yr (most <0.05 GtN/yr) for PU and <0.03 GtN/yr (most <0.01 GtN/yr) for BNF. The largest PU emulation error is found for

ACCESS-ESM1-5 (up to ±0.15 GtN/yr). For most ESMs in the hist_ssp and 1pctCO2-bgc experiments, mean emulation errors remain within ±0.01 GtN/yr for PU and ±0.004 GtN/yr for BNF. Given that PU ranges from 0.35 to 2.5 GtN/yr (mostly 0.6–1.5 GtN/yr) and BNF ranges from 0.025 to 0.23 GtN/yr across the studied ESMs, these small mean errors highlight the effectiveness of the updated CNit parameterizations in capturing these fluxes. In the 1pctCO2 experiment, larger PU overestimations are observed for the two CMCC models, MIROC-ES2L, NorESM2-LM, UKESM1-0-LL, and CESM2-WACCM (mean errors of 0.02–0.05 GtN/yr), while a PU underestimation of approximately 0.025 GtN/yr is found for MPI-ESM1-2-LR. BNF is also overestimated for ACCESS-ESM1-5 and MIROC-ES2L (0.008–0.025 GtN/yr) and underestimated for the two NorESM models (∼0.02 GtN/yr) in their 1pctCO2 simulations.

For nitrogen states, the CNit emulation of N_{Lando} performs better in the hist_ssp series and 1pctCO2-bgc experiments than in the 1pctCO2 experiment. The absolute error is smaller than 2.5 GtN (mean error mostly within ±0.3 GtN) in the former, while it can reach approximately −5.0 GtN in the latter for ACCESS-ESM1-5, NorESM2-LM, and CESM2-WACCM (mean error between −1.7 and −2.1 GtN). This negative bias persists throughout the 1pctCO2 experiment. The N_M is less well emulated than the N_{Lando}, with the largest error found for ACCESS-ESM1-5 under the hist_ssp experiments (persistent overestimation with a mean of ∼3.0 GtN). Larger emulation errors are also seen for the two NorESM models and CESM2-WACCM, with mean errors within −0.5 to −1.0 GtN (underestimations). These models feature larger N_M pools than the others—∼36.0 GtN for ACCESS-ESM1-5, ∼6.0 GtN for the NorESM models, and <4.0 GtN for the rest. There are overestimations in the emulated nNetLand, which shows persistent positive bias for ACCESS-ESM1-5, the two NorESM models, and CESM2-WACCM (mean errors of ∼0.05, ∼0.015, and ∼0.01 GtN/yr, respectively). In contrast, N_M and nNetLand emulation errors from the 1pctCO2 and 1pctCO2-bgc experiments show underestimations, with a mean of <1.5 GtN for N_M and <0.015 GtN/yr for nNetLand in most ESMs.

This N_M emulation is a model limitation since CNit v1.0 (Tang, Nicholls, Norton, et al., 2025). The current emulation error is comparable to the previous one. For ACCESS-ESM1-5, the error is even larger than the others (note that this model was not included in the prior calibration). Potential causes were discussed in the CNit v1.0 calibration (Tang, Nicholls, Norton, et al., 2025). On the parametrization side, we revised the N_M turnover formulation to separately represent gaseous and leaching losses (Equation 26). However, due to the lack of data on the different forms of mineral nitrogen loss, this enhanced model capability was not utilized in the current calibration (see Section 3.2). As a result, the formulation limitation presents in CNit v1.0 remains. A key difference in this calibration is the consistent use of AFOLU nitrogen emissions (as nLUmin) and LUH2 fertilizer application (as FT) as inputs for CNit v2.0 (see Section 3.2 for the justification), rather than ESM outputs used in the previous calibration. The LUH2 fertilizer application flux increases from zero (before the 1910s) to 0.1–0.2 GtN/yr by 2100 (Figure A1), depending on the SSP scenarios, which is a large flux compared to atmospheric deposition (<0.08 GtN/yr for all SSP scenarios). Since FT directly enters the N_M (Figure 1), the discrepancy arises if the ESMs do not use LUH2 FT in their simulations, while we do in our calibration. Consequently, N_M overestimation primarily occurs in the hist_ssp experiments, but not in the 1pctCO2 and 1pctCO2-bgc experiments (Figure 2), where FT is set to zero to reflect pre-industrial conditions. To enhance the CNit simulation of N_M, we suggest that future CMIP ESMs adopt more consistent nitrogen fertilizer input data and report gaseous and leaching losses separately. This would allow CNit to use the same inputs as the ESMs and test updated NM turnover parameterizations. Nevertheless, given the much smaller size of N_M compared to organic nitrogen pools (<1 GtN vs. >100 GtN), the emulation error is unlikely to substantially affect estimates of total land nitrogen dynamics.

For some models, the emulation exhibits systematic bias in the 1pctCO2 and 1pctCO2-bgc experiments, but not in the hist_ssp experiments (for both carbon and nitrogen variables). This occurs because model behavior with or without land use change forcings can differ substantially in ESMs. Such non-linearity, driven by regional differences or underlying physical processes, presents a challenge for CNit, which aims to capture all dynamics within a simplified global annual-mean framework (see Section 3.3). Future updates to CNit's land use representation are expected to improve performance in these idealized experiments.

5. Carbon–Nitrogen Cycle Dynamics and Process Attribution in CNit Emulations

The following results and discussions focus on the varying responses of processes to CO_2 concentration, climate, and nitrogen status, as diagnosed from the process-based CNit emulation (despite the use of highly parameterized

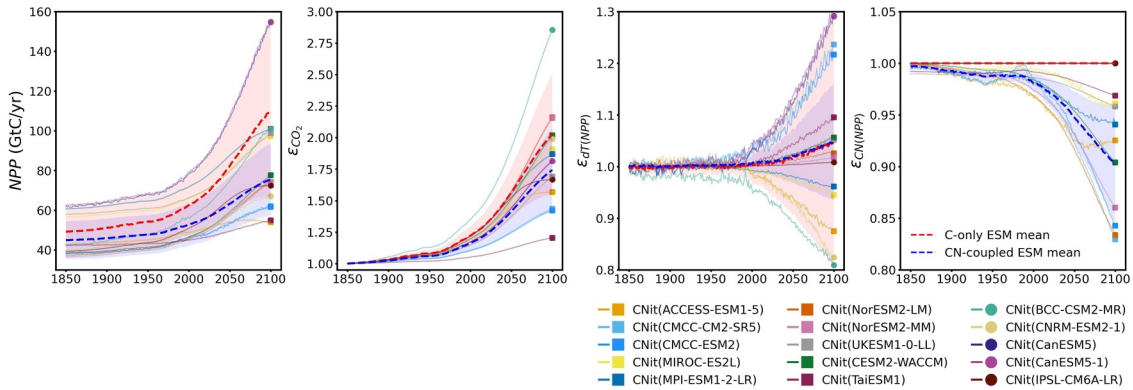

Figure 3. The emulated net primary production (NPP) and its response to CO_2 fertilization (ϵ_{CO_2}), temperature change ($\epsilon_{dT(NPP)}$), and carbon-nitrogen coupling ($\epsilon_{CN(NPP)}$) for CMIP6 ESMs under the hist_ssp585 experiment. The dashed lines represent the multi-model mean values (red: C-only ESMs; blue: CN-coupled ESMs). The shaded areas indicate the multi-model mean ± 1 standard deviation ranges (red: C-only ESMs; blue: CN-coupled ESMs).

process representations). Detailed calculations for updated processes are provided in Section 2. Calculations unchanged from CNit v1.0, such as the CO_2 fertilization and temperature effects, are provided in Tang, Nicholls, Norton, et al. (2025). Since all experiments are calibrated simultaneously using a single set of best-estimate parameters for each ESM (see Section 3.3), we present results from the hist_ssp585 experiment as an illustrative example. The diagnosed effects and responses in the other experiments show broadly similar trends to their corresponding drivers (Figure A1), consistent with the exponential formulations (e.g., Equations 24 and 25). We reiterate that the effects parameterized in the CNit emulation—represented as unitless scalars quantifying the responses of processes to various factors—are based on global annual-mean values.

5.1. The CO2 Fertilization, Climate Response, and Carbon-Nitrogen Coupling Effects on NPP

The emulated NPP for the C-only ESMs shows larger variability compared to the CN-coupled ESMs (67.2–156.5 vs. 54.0–101.0 GtC/yr in 2100, Figure 3). Among all the ESMs studied, the NPP emulated for the two CanESM models maintains the highest values and shows a large increase across the entire period (from 62.2 to 156.5 GtC/yr), whereas the NPP emulated for ACCESS-ESM1-5 and TaiESM1 shows much smaller starting values and increases (from 42.2 to 54.9 GtC/yr). The multi-model mean NPP increases for both the C-only and CN-coupled ESMs, with the former consistently showing higher values (49.3–110.4 vs. 44.9–75.6 GtC/yr). Additionally, NPP accelerates faster in the C-only ESMs starting around 2000. The above also reflects the original ESM outputs, given the close match between the CNit emulations and the ESM-simulated NPP (Figure 2).

From the CNit parameterization, the multi-model mean CO_2 fertilization effect (ϵ_{CO_2}) is larger in the C-only ESMs than in the CN-coupled ESMs, with an expanding difference in the future (ϵ_{CO_2} of 2.03 ± 0.48 vs. 1.74 ± 0.33 in 2100), explaining the more rapid NPP increase in the C-only ESMs. There is an outlier high ϵ_{CO_2} of 2.86 in 2100 for BCC-CSM2-MR. If excluding an outlier C-only ESM, BCC-CSM2-MR, the multi-model mean ϵ_{CO_2} for the C-only ESMs becomes 1.82 ± 0.13 in 2100, which is less variable but remains larger than that of the CN-coupled ESMs. This is in line with previous findings that demonstrate the overlap of carbon-concentration feedbacks between C-only and CN-coupled ESMs (Arora et al., 2020).

The emulated temperature response of NPP is similar for both the C-only and CN-coupled ESMs (multi-model mean $\epsilon_{dT(NPP)}$ of 1.05 in 2100 for both groups), though it shows greater variability for the C-only ESMs. The strongest negative climate response of NPP is found for BCC-CSM2-MR ($\epsilon_{dT(NPP)}$ of 0.80 in 2100, i.e., 20% reduction of NPP), while a large enhancement of NPP with warming is found for the two CanESM models ($\epsilon_{dT(NPP)}$ of 1.30 in 2100). All these models are C-only, which contributes to the large spread in the results. The strong negative climate response in BCC-CSM2-MR counters its high CO_2 fertilization, leading to a moderate increase in NPP across the hist_ssp585 period (43.1–101.1 GtC/yr). The high $\epsilon_{dT(NPP)}$ combined with the moderate ϵ_{CO_2} in the two CanESM models are responsible for their nearly tripled NPP increase from 1850 to 2100.

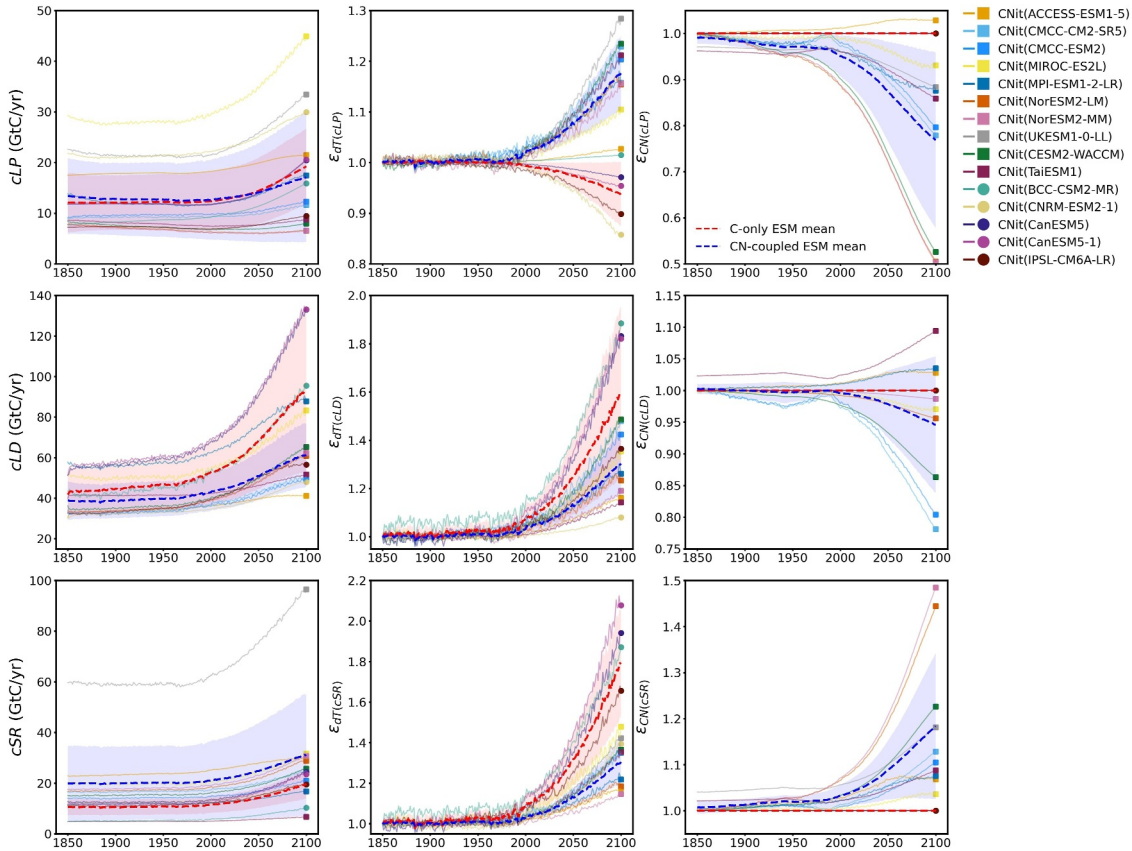

Figure 4. The emulated carbon turnover processes, including litter production (cLP), litter decomposition (cLD), and soil respiration (cSR), and their responses to temperature change (ϵ_{dT}) and carbon-nitrogen coupling (ϵ_{CN}) for CMIP6 ESMs under the hist_ssp585 experiment. The dashed lines represent the multi-model mean values (red: C-only ESMs; blue: CN-coupled ESMs). The shaded areas indicate the multi-model mean ± 1 standard deviation ranges (red: C-only ESMs; blue: CN-coupled ESMs).

The carbon-nitrogen coupling effect on NPP ($\epsilon_{CN(NPP)}$) consistently indicates nitrogen limitation across the CN-coupled ESMs throughout the hist_ssp585 period (i.e., a nitrogen deficit). This limitation increases over time for most ESMs, with $\epsilon_{CN(NPP)}$ ranging from a minimum of 0.83 (CMCC-CM2-SR5) to a maximum of 0.97 (TaiESM1) by 2100.

5.2. The Climate Response and Carbon-Nitrogen Coupling Effect on Carbon Turnovers

The multi-model mean cLP for both groups is very similar, increasing from ∼12.0 to ∼18.0 GtC/yr during the hist_ssp585 period (Figure 4). The emulated cLP for the C-only ESMs shows less variability compared to the CN-coupled ESMs, with a standard deviation of 7.5 versus 12.9 GtC/yr in 2100. The emulated cLP for MIROC-ES2L shows the highest values throughout the entire period, increasing from 29.2 to 33.4 GtC/yr. Interestingly, from a multi-model mean perspective, the emulated temperature response of cLP shows opposite signs between the C-only ESMs (−6.5%) and CN-coupled ESMs (+15.6%). The nitrogen deficit inhibits litter production by an average of 23.1% in 2100. The strongest limitation is found for the two NorESMs (∼50.0% reduction), while a slight enhancement in cLP is observed for ACCESS-ESM1-5 (2.8%).

During the experimental period, the emulated cLD for the C-only ESMs increases from 41.7 ± 10.0 to 93.7 ± 41.2 GtC/yr, while for the CN-coupled ESMs, it increases from 35.0 ± 15.2 to 55.2 ± 24.4 GtC/yr. The highest cLD is observed for the two CanESM models (∼133.0 GtC/yr in 2100), which correlates with their high NPP (the highest among the studied ESMs, Figure 3). Their elevated cLD is driven by a strong temperature response (>80.0% enhancement of cLD in 2100). The highest warming-enhanced cLD is found for BCC-CSM2-MR (88.5% in 2100), concurrent with its highest CO_2 fertilization effect and strongest negative climate response of NPP (Figure 3). These responses yield a multi-model mean temperature response of cLD of 1.60 ± 0.36 for the C-only

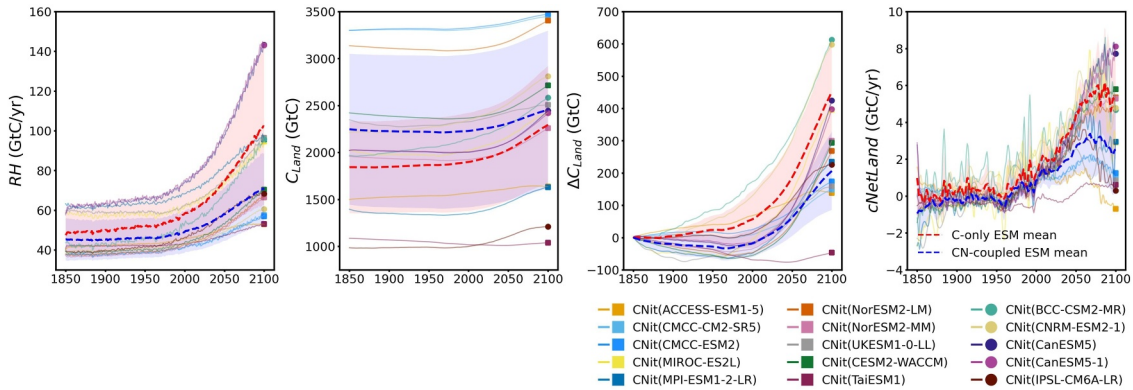

Figure 5. The emulated heterotopic respiration (RH), land carbon pool size (C_{Land}), land carbon uptake (ΔC_{Land}), and net land carbon flux (cNetLand) for CMIP6 ESMs under the hist_ssp585 experiment. The dashed lines represent the multi-model mean values (red: C-only ESMs; blue: CN-coupled ESMs). The shaded areas indicate the multi-model mean ± 1 standard deviation ranges (red: C-only ESMs; blue: CN-coupled ESMs).

ESMs in 2100, compared to 1.30 ± 0.14 for the CN-coupled ESMs (i.e., an average cLD enhancement of 60.0% vs. 30.0%). The multi-model mean nitrogen effect on litter decomposition is limiting the process ($\epsilon_{\text{CN(cLD)}}$ = 0.95 ± 0.11 in 2100) but this is model-dependent, as ACCESS-ESM1-5, MPI-ESM1-2-LR, and TaiESM1 show an enhancement of litter decomposition due to the nitrogen effect (<10.0% in 2100).

Most emulated cSR values range from 10.0 to 30.0 GtC/yr. The lowest and highest cSR values are found for TaiESM1 (from 4.8 to 6.7 GtC/yr) and UKESM1-0-LL (from 59.7 to 96.5 GtC/yr), respectively. The emulated cSR for C-only ESMs is consistently lower than for CN-coupled ESMs (~10.0 GtC/yr lower on average), yet their climate response is stronger (mean $\epsilon_{dT(\text{cSR})}$ 1.79 vs. 1.30 in 2100). The strongest climate response in soil respiration is found for the two CanESM models, with an approximately doubled increase by 2100 ($\epsilon_{dT(\text{cSR})}$ of 1.94 and 2.08, respectively). The nitrogen effect is increasing soil respiration, with the largest enhancements of 44.4% and 48.4% for NorESM2-LM and NorESM2-MM, respectively. Other models show $\epsilon_{\text{CN(cSR)}}$ values ranging from 1.03 to 1.23, resulting in a multi-model mean of 1.18 ± 0.16 in 2100.

5.3. The Heterotrophic Respiration, Land Carbon State, and Net Land Carbon Flux

The emulated RH shows clear differences between the C-only and CN-coupled ESMs, with the former consistently exhibiting higher values (Figure 5). Overall, RH follows similar trends to those of NPP (Figure 3), which is expected, as their difference determines the cNetLand (i.e., net biosphere production). This flux should be similar across all ESMs, particularly during the historical period. It also suggests that if a model overestimates one component, the other is likely to be overestimated as well (e.g., the extremely high NPP and RH in the two CanESM models).

The initial C_{Land} varies substantially among ESMs, ranging from 984.6 GtC in IPSL-CM6A-LR to 3300.3 GtC in CMCC-ESM2 (Figure 5). The multi-model mean emulated C_{Land} is consistently smaller for the C-only ESMs than for the CN-coupled ESMs throughout the entire hist_ssp585 period. However, the emulated C_{Land} shows a larger increase during the scenario phase for the C-only ESMs, resulting in total carbon uptake (ΔC_{Land}) of 451.8 ± 159.8 GtC and 206.5 ± 121.1 GtC for the C-only and CN-coupled ESMs, respectively. In the historical period, the emulated C_{Land} decreases (i.e., negative cNetLand) for the CN-coupled ESMs, a pattern not observed for the C-only ESMs based on their multi-model means. The mean cNetLand remains consistently higher for the C-only ESMs than for the CN-coupled ESMs, with the difference widening in the scenario phase (2.5 ± 2.3 vs. 5.1 ± 3.1 GtC/yr in 2100).

5.4. The Biological Nitrogen Fixation, Land Nitrogen State, and Net Land Nitrogen Flux

The emulated BNF increases across most of the ESMs during the hist_ssp585 period (Figure 6). The multi-model mean increases from 0.086 ± 0.047 to 0.157 ± 0.033 GtN/yr, with a sharp increase beginning in the 1950s. The highest BNF occurs in ACCESS-ESM1-5, which remains above 0.175 GtN/yr throughout the period. However, it

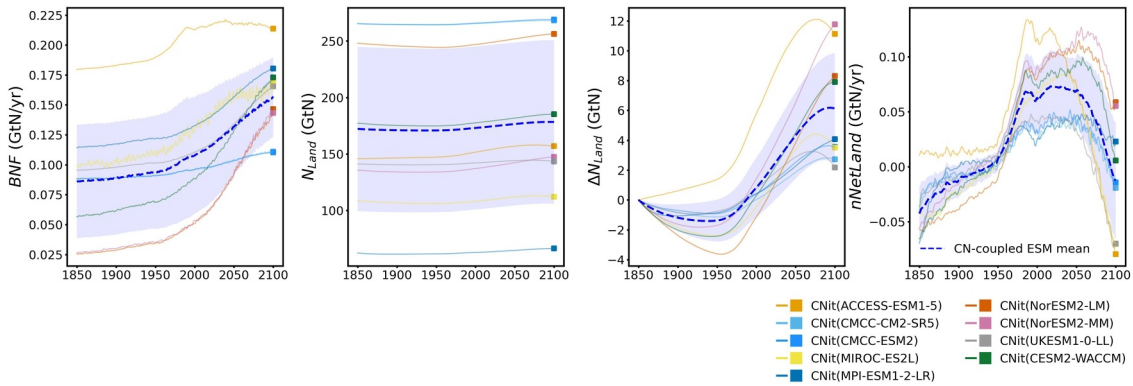

Figure 6. The emulated biological nitrogen fixation (BNF), land nitrogen pool size (N_{Land}), land nitrogen uptake (ΔN_{Land}), and net land nitrogen flux (nNetLand) for CMIP6 ESMs under the hist_ssp585 experiment. The dashed lines represent the multi-model mean values (CN-coupled ESMs). The shaded areas indicate the multi-model mean ± 1 standard deviation ranges (CN-coupled ESMs).

first plateaus at ~0.210 GtN/yr (around 2000s), then flattens before slightly declining. These patterns are also observed in the original ESM outputs, as BNF is well emulated by CNit (Figure 2).

The emulated N_{Land} shows considerable variation throughout the period, with its multi-model mean increasing by ~11.0 GtN during the hist_ssp585 period (from 172.2 ± 72.6 to 183.2 ± 73.6 GtN, Figure 6). The largest emulated N_{Land} values are found for the two CMCC models and NorESM2-LM, which are more than three times larger than the smallest N_{Land} observed in MPI-ESM1-2-LR (>250.0 vs. <70.0 GtN).

The emulated land nitrogen accumulation (ΔN_{Land}) shows an increasing spread after 1950, with the standard deviation reaching 8.2 GtN in 2100 (compared to a mean of 11.0 GtN). The largest ΔN_{Land} is emulated for ACCESS-ESM1-5 and the two NorESM models, ranging from 10.0 to 18.0 GtN in 2100. In contrast, the smallest ΔN_{Land} is emulated for UKESM1-0-LL and MIROC-ES2L (2.4 and 3.8 GtN), both of which show a decreasing trend in the later phase of the ssp585 scenario.

Similar to ΔC_{Land}, ΔN_{Land} shows a decreasing trend before 1950 due to negative nNetLand. However, the decrease in nNetLand after 2050 is much more rapid than that of cNetLand (from a multi-model mean perspective). The emulation for both UKESM1-0-LL and MIROC-ES2L show negative cNetLand in 2100 (i.e., net land nitrogen emission, ~0.07 GtN/yr).

6. Discussion

6.1. Overestimation of NPP in CMIP6 ESMs—The Role of CO_2 Fertilization

The overestimation of historical GPP in CMIP5 and CMIP6 C-only ESMs (compared to observations and reanalysis data sets for 1986–2005) has been extensively reported in previous studies (Anav et al., 2013; Gier et al., 2024), with this bias attributed to the absence of nitrogen cycle representation in these models. A similar positive bias in modeled NPP (compared to observations) from CMIP6 ESMs has been observed, although smaller than that seen in CMIP5 models (e.g., ~12% vs. ~31%, for 2001–2005, values from Varney et al. (2022) and Wei et al. (2022). This overestimation of both GPP and NPP persists into the more recent period (2000–2014), with biases of 16% and 13%, respectively, as reported by Hu et al. (2022). Our results also reveal a notably higher NPP in the C-only ESMs, with a more pronounced acceleration during the scenario period (Figure 3, consistent with the ESM outputs), suggesting that these models continue to overestimate NPP, particularly under high-emission future scenarios.

Although the inclusion of the nitrogen cycle is a key factor in explaining the more constrained NPP in CN-coupled ESMs (Anav et al., 2013; Davies-Barnard et al., 2020; Gier et al., 2024), our emulation shows that the CO_2 fertilization effect (on average, 29% stronger in C-only ESMs than in CN-coupled ESMs, Figure 3) plays a larger role than nitrogen limitation on NPP (on average, 10%). Given that the mean climate response is nearly identical for both C-only and CN-coupled ESMs, this suggests that, from a global annual-mean perspective, the over-represented CO_2 fertilization sensitivity has a greater impact on NPP overestimation than nitrogen cycle inclusion

(i.e., incorporating the nitrogen cycle may not sufficiently offset the overestimation of CO_2 fertilization effect). Excluding the extreme CO_2 fertilization sensitivity in BCC-CSM2-MR, the 8% difference in CO_2 fertilization remains comparable to the difference observed between ESMs with or without a nitrogen cycle, highlighting the critical role of accurately representing NPP sensitivity to elevated CO_2 (Kolby Smith et al., 2016; Schimel et al., 2015). Consequently, the current carbon-concentration feedback in ESMs may be overestimated (Arora et al., 2020).

Experiments show that NPP and biomass accumulation responses to CO_2 enrichment vary depending on ecosystem type and age (Jiang et al., 2020), but models struggle to capture these differences effectively (Walker et al., 2019). A recent study focusing on the period 1982–2015 reports a declining trend in the CO_2 fertilization effect in models, although this trend is substantially weaker than that observed (Wang et al., 2020). This underrepresentation is likely due to model limitations in simulating nutrient constraints (He et al., 2017), soil water availability (and water use efficiency) (Li et al., 2021), regional disparities (McGrath & Lobell, 2013), and their combined effects (Zhang et al., 2022). The overestimation of GPP and leaf area index in Sub-Saharan Africa and the United States, and their underestimation in Northeastern South America, are persistent model biases since CMIP5 for both C-only and CN-coupled ESMs (Gier et al., 2024), indicating that future model development should devote greater attention to CO_2 fertilization strength in these regions. These results further support the need for refinement of CO_2 fertilization representations in ESMs. Nevertheless, there remains considerable variability in the climate response of NPP across CMIP6 ESMs, both in global annual-mean values (Figure 3) and spatial patterns (e.g., tropical vs. extratropical regions, (Zhu et al., 2022)). Thus, climate response cannot be entirely disregarded when comparing the relative strength of different effects across individual models.

A key limitation of the current calibration, as well as our previous calibration (Tang, Nicholls, Norton, et al., 2025), is the lack of C-only reference simulation results from the CN-coupled ESMs. In other words, direct constraints on the emulated nitrogen effect on NPP are unavailable. However, several factors increase our confidence in the emulated nitrogen effect on NPP.

First, the emulated carbon-nitrogen coupling effect on NPP is comparable to results from many land surface models running C-only and CN-coupled experiments. For example, JULES-CN (the land component in UKESM, Table 1) in the RCP8.5 scenario show a ∼6% reduction in NPP in 2100 in the CN-coupled mode compared to the C-only mode (estimated from Huntingford et al. (2022)). There is a 12.7% NPP reduction from O-C to O-CN in the historical simulation (1860–2002) (Zaehle et al., 2010), and a ∼10% reduction in NPP from its C-only reference to O-CN's 30 model ensemble (with various representations for C:N flexibility, BNF, ecosystem nitrogen loss, and their combinations) at the end of their RCP8.5 and RCP2.6 scenario runs (Meyerholt et al., 2020). JSBACH shows a smaller NPP reduction (∼10%) by CN-coupling over the entire 1pctCO2 scenario period (Goll et al., 2017). Similarly, the MIT Integrated Global Systems Model (IGSM) shows comparable nitrogen limitations on both GPP and autotrophic respiration (Sokolov et al., 2008). Some models, however, report much larger NPP reductions in CN-coupled mode, such as a 15%–45% reduction in different CN-coupled schemes (TECO-CN, CLM 4.5, and O-CN) compared to the TECO-C mode during the Duke Forest simulation from 1996 to 2007 (Du et al., 2018). Some models report more than ∼50% NPP reductions, such as an early version of CLM-CN (CLM v3.0 + Biome-BGC v4.1.2) during the later phases of the SRES A2 scenarios (Thornton et al., 2007), or the CABLE model in 2100 under RCP8.5 (Fleischer et al., 2019). These large differences highlight the significant uncertainty in carbon-nitrogen coupling. Nonetheless, a >50% nitrogen limitation on global NPP is unlikely unless the NPP simulated in the C-only mode is excessively high. This suggests the possibility of overly strong CO_2 sensitivity in these models, which further support our emulation results (Figure 3).

Second, the inclusion of the 1pctCO2 and 1pctCO2-bgc simulations in our calibration allows us to disentangle the climate response and CO_2 fertilization effects. The ≥4 SSP scenarios, with their wide range of co-varying CO2 concentrations and temperatures, further constrain both the CO_2 fertilization and climate effects. If the CO_2 fertilization effect and temperature response are validated, this will indirectly constrain the emulated nitrogen effect.

Finally, the historical period is calibrated for both C-only and CN-coupled ESMs. Since the historical NPP increase is similar across the ESMs, this also serves as an indirect constraint on the emulated nitrogen effect.

6.2. Turnover-Driven Divergence of Land Carbon Dynamics in CMIP6 ESMs

The C-only ESMs exhibit both higher NPP and RH compared to the CN-coupled ESMs (Figures 3 and 5). However, these changes are not proportional, leading to higher estimates of land carbon uptake and net biosphere production in the C-only ESMs (Figure 5). The inclusion of the nitrogen cycle and nitrogen availability are key factors driving these differences (Kou-Giesbrecht et al., 2023; Zaehle et al., 2015).

When breaking it down into processes, our emulation shows that the difference arises not only from NPP and the effects on it (Figure 3), but also from nearly all turnover fluxes and their responses to climate and nitrogen availability (Figure 4).

First, the turnover fluxes differ substantially across ESMs. In 1850, the maximum cLP and cSR fluxes are about three times their respective minima, reflecting differences in initial carbon pool sizes (Figure 5). A comparison with observations reveals both overestimations and underestimations of soil and litter carbon by CMIP6 ESMs (Varney et al., 2022), highlighting the significant uncertainty in the modelled soil and litter carbon states.

Second, the climate response of cLP is opposite in the C-only and CN-coupled ESMs (Figure 4). The similar multi-model mean cLP in both C-only and CN-coupled ESMs results from the simultaneous positive climate response and nitrogen limitation in the CN-coupled ESMs (in contrast to the negative climate response in the C-only ESMs), highlighting the importance of nitrogen inclusion. The warming-induced vegetation shift leading to ecological drought contributes to the positive climate response of cLP (Tietjen et al., 2017). Nitrogen limitation on litter production aligns with the community-level leaf lifespan's dependence on nutrient availability, with longer leaf lifespan communities in nutrient-poor environments maximizing nitrogen use efficiency (Aerts & Chapin, 1999; Pornon et al., 2011; Reich et al., 1997). Without this consideration, the C-only ESMs may misattribute nitrogen limitation to the negative climate response. Overall, the cLP in CMIP6 ESMs shows a negative response (within ∼10% inhabitation, i.e., slowing plant mortality and/or leaf shedding) to the combined climate and nutrient conditions in the hist_ssp585 period. Nutrient limitation, warming-induced precipitation increases (Trenberth, 2011), warming-altered leaf senescence (Zohner et al., 2023), and the shift in productivity allocation to belowground (Liu et al., 2018) contribute to this global annual-mean response.

Lastly, the climate response of cLD and cSR in the C-only ESMs is higher than in the CN-coupled ESMs (multi-model mean values, Figure 4), but still insufficient to offset their high NPP (Figure 3). The cLD (fraction to atmosphere, cLD2A, i.e., litter respiration and labile soil organic matter decomposition) and cSR are component fluxes of RH (Equation 4). The cLD2A contributes 40%–90% of RH except for UKESM-0-LL, which lacks a litter pool. Comparatively, the cLD2A in the C-only ESMs shows a higher contribution than in the CN-coupled ESMs (with lower cSR and higher RH in the C-only ESMs, Figures 4 and 5). This suggests that the climate response of cLD is underestimated in the C-only ESMs, as it is not sensitive enough to respire the excessively high NPP. Given the multi-model mean nitrogen effect in limiting cLD, nitrogen inclusion further differentiates cLD between the C-only and CN-coupled ESMs, explaining the lower RH increase in the CN-coupled ESMs (Figure 5). The global nitrogen effect on litter decomposition remains inconclusive, with litter quality and climate as the primary factors influencing the decomposition rate (Knorr et al., 2005; Krishna & Mohan, 2017; Mcclaugherty et al., 1985). This suggests that the emulated nitrogen effect is a global aggregation of multiple factors, explaining its variability across CMIP6 ESMs.

For the cSR, the climate effect in the C-only ESMs is ∼1.5 times that in the CN-coupled ESMs, suggesting a potential misattribution of nitrogen effects in the climate response of the C-only ESMs (similar to cLP, Figure 4). A recent study examining land carbon cycle feedbacks indicates that soil carbon-climate feedback dominates land carbon-climate feedback in CMIP6 ESMs (Varney et al., 2024). Our results underscore the necessity of further disentangling nitrogen cycle feedbacks to accurately estimate carbon-cycle feedbacks (Kou-Giesbrecht et al., 2025; Ziehn et al., 2021).

In the studied CN-coupled ESMs, nitrogen deficit consistently stimulates cSR to a degree comparable to its climate response (Figure 4), which contrasts with the nitrogen limitation effect observed for cLD in the multi-model mean. Observations of reduced soil respiration following nitrogen enrichment in forest soils (Janssens et al., 2010; Sun et al., 2014; Zeng et al., 2023) partially support this nitrogen deficit–induced enhancement of cSR. Contributing factors include changed carbon availability (Eberwein et al., 2015), increased recalcitrant

carbon utilization (Zeng et al., 2023), and enhanced below-ground carbon allocation (Janssens et al., 2010). The latter is consistent with the emulated nitrogen limitation on cLP. In our emulation, nitrogen deficit reflects the imbalance between plant nitrogen demand and availability (Equations 17–19), serving as an indicator of ecosystem nitrogen status. However, this does not necessarily imply a nitrogen deficit for litter and soil organic matter decomposition. For the whole system, the reduced nitrogen plant uptake under deficit conditions may increase nitrogen availability for microbial communities, thereby enhancing cSR. The divergent climate responses and nitrogen effects on cLD and cSR largely contribute to the differences in RH between the C-only and CN-coupled ESMs (Figure 5).

6.3. Variability of Land Nitrogen Dynamics in CMIP6 ESMs

There is significant spread in both BNF and land nitrogen dynamics in the emulation results (Figure 6, consistent with the ESM outputs). Despite the more constrained NPP in the CN-coupled ESMs during the historical period (Figure 3), the spread in BNF is larger in the historical period than in the scenario period (standard deviation of 0.047 GtN/yr in 1850 vs. 0.033 GtN/yr in 2100, Figure 6). Compared to NPP (Figure 3), the emulated BNF also exhibits more diverse trends among models in the scenario period (Figure 6). As the largest natural land nitrogen input, BNF is a key flux influencing model-based estimates of net land carbon uptake (Meyerholt et al., 2016). However, neither observational data nor current model representations provide a consistent and high-confidence global estimate of BNF (Davies-Barnard et al., 2022; Davies-Barnard & Friedlingstein, 2020; Vitousek et al., 2013). Globally, there is no uniform relationship between BNF and NPP —BNF:NPP ratios vary across models, showing increases, decreases, or no change (Figure A2)—nor between N_{Land} and C_{Land} (Figure A2).

All ESMs, except ACCESS-ESM1-5, simulate an increasing land N:C ratio during the historical period (Figure A2), followed by a decline in the scenario period. Considering that both carbon and nitrogen accumulate on land during the scenario period (Figures 5 and 6), the declining N:C ratio indicates that nitrogen loss is more sensitive to future climate than carbon. This aligns with our emulated temperature sensitivity of nitrogen loss, which shows a 1.4–2.5-fold amplification of initial nitrogen loss (Figure A3). Historical overestimation of nitrogen loss from denitrification—nearly twice the isotope-based estimates—has been reported (Feng et al., 2023), suggesting that high climate sensitivity may further accelerate nitrogen loss in the future due to accumulated nitrogen in the historical period being more prone to volatilization.

Nitrogen addition experiments using offline land surface models from CMIP6 ESMs reveal diverse responses in BNF, nitrogen use efficiency, and various components of the land nitrogen budget (Davies-Barnard et al., 2020). These differences align with the varied changes in land nitrogen pool sizes and net land nitrogen fluxes (Figure 6). Our emulation of nitrogen turnover fluxes shows that most of the uncertainty arises from nLP, based on the relative variability among ESMs (standard deviation-to-mean ratios of 0.60, 0.41, 0.40, and 0.20 for nLP, nLD, nSR, and nLS, respectively; Figure A3). While the multi-model mean trends of climate and nitrogen responses in nitrogen turnover processes resemble those of their carbon counterparts, the inter-model spread is larger—particularly for soil respiration (Figure A3).

7. Comparison With CNit v1.0 Calibration and Insights for Future RCM Calibration Strategies

In CNit v2.0 and its calibration, we have addressed three major limitations from our previous work (Tang, Nicholls, Norton, et al., 2025): the explicit parameterization of nitrogen status, the inclusion of BNF simulation, and the disentangling of climate response and carbon-nitrogen coupling effects. The first two improvements are related to updated parameterizations, while the third is a calibration setup enhancement (by incorporating 1pctCO2 and 1pctCO2-bgc scenarios in the calibration). Additionally, we have updated the parameterization for nitrogen loss flux simulation and improved the separation of anthropogenic nitrogen emissions between the mineral and organic pools, aiming to enhance the emulation of the mineral nitrogen pool size. However, the dynamics of the mineral nitrogen pool size remain relatively less well emulated (Figure 2). There are mainly two reasons: (a) we have applied consistent AFOLU land use emissions and LUH2 nitrogen fertilization inputs for CNit v2.0, which may differ from the ESM-simulated land use emissions and fertilizer applications; and (b) we have not yet applied the new nitrogen loss formulation that separates gaseous and leaching losses in the current

calibration, limited by data availability in the studied ESMs and the mass conservation issues in the existing data (Tang, Nicholls, Jones, et al., 2025). The latter should become more accessible in the future as ESMs couple the land nitrogen cycle with the atmosphere and ocean, where the separation of gaseous and leaching losses is essential.

Using AFOLU, LUH2, or other scenario-based emissions as input for the CNit calibration—while it may undermine calibration performance (in general, not just for mineral nitrogen dynamics)—is suggested to become a standard approach in calibrating RCMs' carbon and nitrogen cycles. This is because emission scenarios in RCM applications are derived from Integrated Assessment Models, which are the sources of the AFOLU and LUH2 data sets. This trade-off is worthwhile because it ensures consistency in both calibration and application, and provides convenience for future applications. This is also supported by our carbon and nitrogen mass conservation analysis of the existing CMIP6 data (Tang, Nicholls, Jones, et al., 2025). When these fluxes are problematic or not available in the published output, it is advisable for users to apply consistent treatment and/or utilize external data sets to ensure fundamental mass conservation.

We recommend that RCMs consider including at least the historical, 1pctCO2, and 1pctCO2-bgc experiments as calibration targets in their carbon cycle calibration. This setup effectively tests RCMs' ability to correctly emulate CO_2 fertilization and climate effects. Moreover, the 1pctCO2 and 1pctCO2-bgc scenarios are commonly used to quantify carbon cycle feedbacks. Calibrating with both would benefit RCM applications in uncertainty quantification of these feedbacks. We also suggest that RCMs use more reliable ESM outputs, including major fluxes (e.g., NPP, RH, BNF, PU, and NetMIN) and all pool sizes, as calibration targets. Along with the utilization of AFOLU and LUH2 data sets, this will allow RCMs to capture key dynamics in the carbon and nitrogen cycles.

8. Conclusions

This paper presents CNit v2.0, with significant advancements in nitrogen deficit representation, BNF, land use emissions, and carbon–nitrogen coupling effect parameterization. CNit v2.0 shows strong emulation of key carbon and nitrogen fluxes and pools across the majority of CMIP6 ESMs, encompassing historical and various idealized and SSP scenario runs (Figure 2).

Emulation of the hist_ssp585 period shows that higher NPP in C-only ESMs relative to CN-coupled ESMs arises from both the absence of nitrogen limitation and a stronger CO_2 fertilization effect. Based on multi-model mean values, nitrogen limitation alone cannot fully compensate the overestimated CO_2 fertilization effect, highlighting the need for re-calibration of the coupled carbon-nitrogen system in the future C-only ESM development. All CN-coupled ESMs show increasing nitrogen limitation on NPP, reaching $10.2 \pm 5.6\%$ inhibition by 2100. The multi-model mean climate response of NPP is positive (warming-enhanced) and similar in magnitude for both C-only and CN-coupled ESMs, though sign-changing uncertainty persists.

Initial land carbon pools vary widely among ESMs (900–3500 GtC). Multi-model mean values indicate that nitrogen deficits relative to plant uptake suppress litter production and decomposition while enhancing soil respiration, although between-model variation remains large. The C-only ESMs may misattribute these nitrogen effects to climate responses. Despite higher climate-driven litter and soil respiration, total heterotrophic respiration in C-only ESMs does not fully counterbalance elevated NPP, leading to overestimated land carbon uptake historically and increasingly in future scenarios compared to CN-coupled ESMs. These results emphasize the importance of nitrogen effect on both NPP and turnover.

Between-model BNF variability is smaller during the scenario period than in the historical period. Both nitrogen turnover and net nitrogen uptake follow trends similar to carbon turnover and net carbon uptake, though with greater variability among ESMs. This corroborates that land acted as a net carbon source before the 1950s and highlights the nitrogen cycle's role in constraining the carbon cycle. During the scenario period, net land nitrogen flux declines faster than net carbon flux, with the multi-model mean turning negative by 2100—indicating that land becomes a net nitrogen source—driven by strong climate-induced nitrogen loss. These results suggest that future nitrogen benefits for carbon storage may be offset by increased nitrogen emissions.

Overall, the diagnosis from CNit emulation demonstrates the significant role of the nitrogen cycle in constraining the carbon cycle, highlighting its importance for broader inclusion in ESMs. The high uncertainty in the current nitrogen cycle underscores the need for further validation. Future work will apply the calibrated CNit v2.0 in probabilistic climate projections using the updated MAGICC-CNit to advance atmospheric CO_2 and climate projections while quantifying carbon and nitrogen cycle feedbacks. Insights and recommendations from the CNit v2.0 calibration are expected to promote greater consistency in future RCM calibrations.

Appendix: Supplementary Figures and Tables

The Appendix provides additional figures and tables to support the descriptions and discussions in the main text (see Figures A1–A3).

(See Table A1).

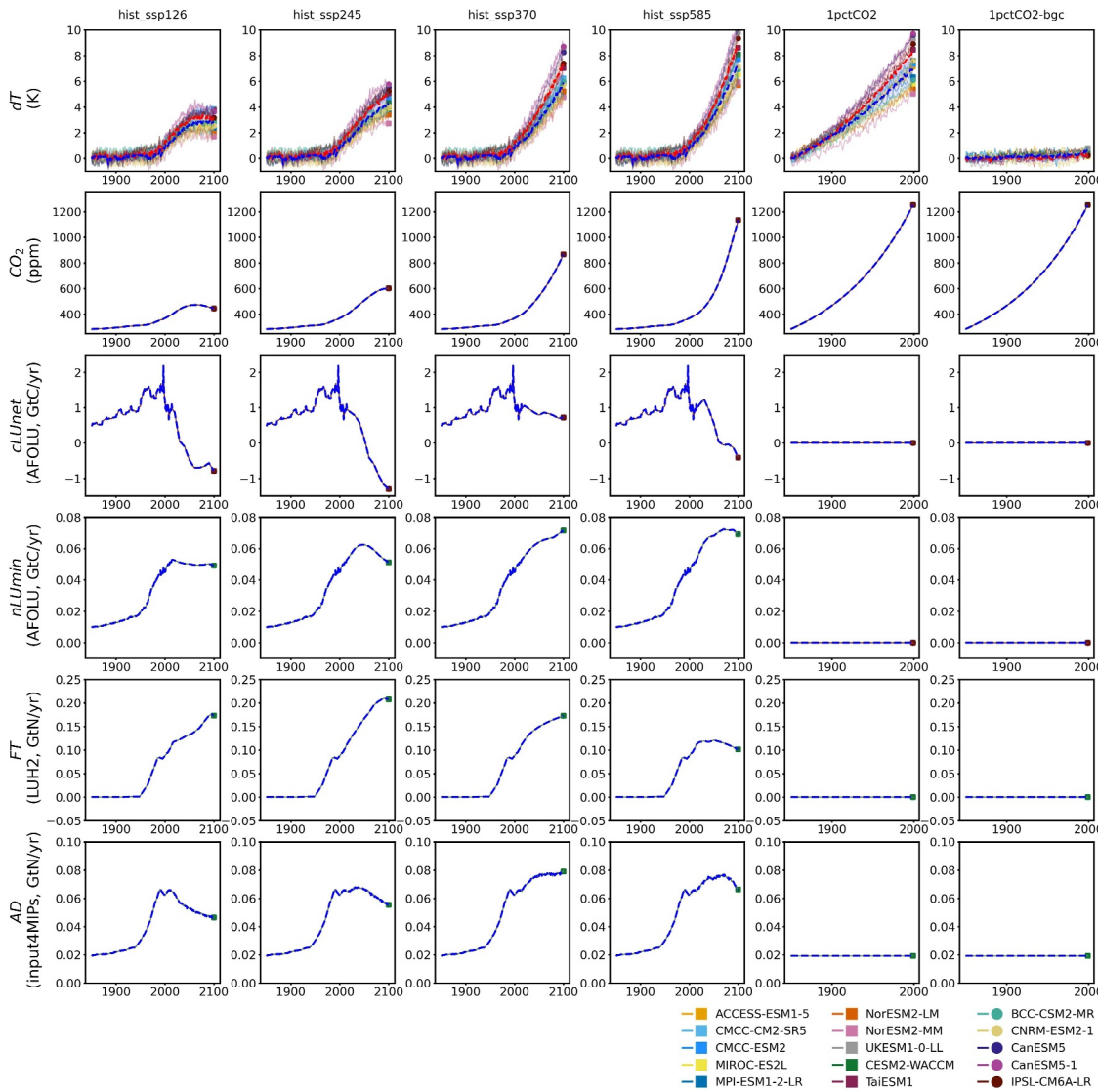

Figure A1. The prescribed temperature change (*dT*, derived from tas in the CMIP6 ESM outputs), atmospheric CO_2 concentration, carbon from land use perturbation as net emission (cLUnet), nitrogen from land use perturbation as mineral nitrogen loss (nLUmin), nitrogen fertilizer application (FT), and atmospheric nitrogen deposition (AD) for calibration. The dashed lines represent the multi-model mean values (red: C-only ESMs; blue: CN-coupled ESMs). The shaded areas indicate the multi-model mean ± 1 standard deviation ranges (red: C-only ESMs; blue: CN-coupled ESMs).

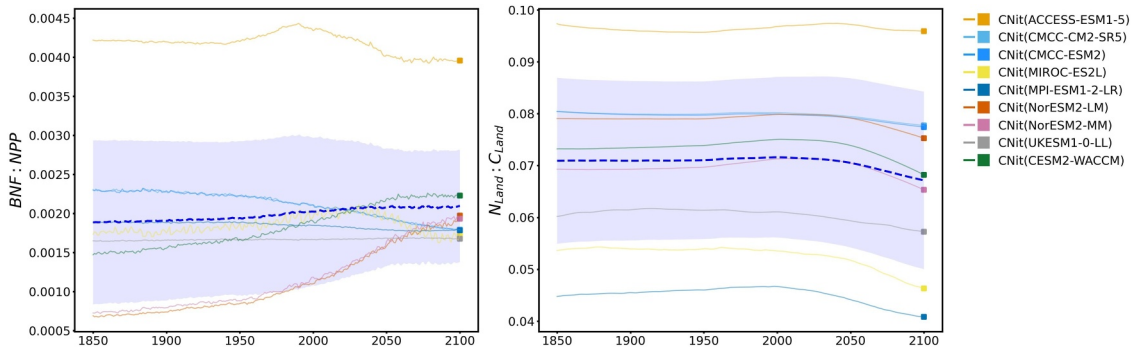

Figure A2. The emulated nitrogen-to-carbon ratios of biological nitrogen fixation (BNF) to net primary production (NPP), and land nitrogen (N_{Land}) to land carbon (C_{Land}). The dashed lines represent the multi-model mean values (CN-coupled ESMs). The shaded areas indicate the multi-model mean ± 1 standard deviation ranges (CN-coupled ESMs).

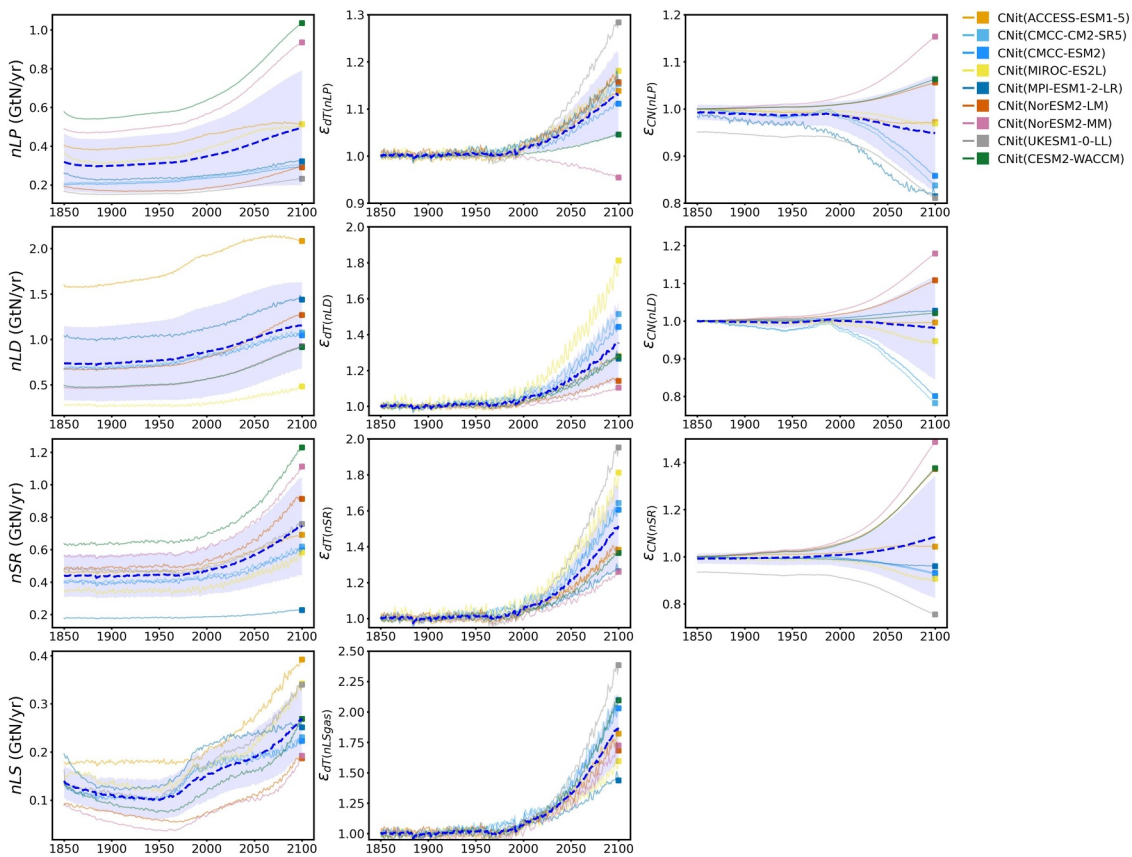

Figure A3. The emulated nitrogen turnover processes, including litter production (nLP), litter decomposition (nLD), soil respiration (nSR), and mineral nitrogen loss (nLS), and their responses to temperature change (ϵ_{dT}) and carbon-nitrogen coupling (ϵ_{CN}) for CMIP6 ESMs under the hist_ssp585 experiment. The dashed lines represent the multi-model mean values (CN-coupled ESMs). The shaded areas indicate the multi-model mean ± 1 standard deviation ranges (CN-coupled ESMs).

Table A1
Target Variables in CNit and Their Corresponding Variable Names in CMIP6

Variable name in CNit	Variable name in CMIP6	Extra information
NPP	npp	Net primary production (calibration target).
RH	rh	Heterotrophic respiration (calibration target).
PU	fNup	Nitrogen plant uptake (calibration target).
BNF	fBNF	Biological nitrogen fixation (calibration target).
NetMIN	fNnetmin	Nitrogen net mineralization (i.e., mineralization - immobilization) (calibration target).
C_P	cVeg	Vegetation carbon pool size (i.e., plant carbon pool size) (calibration target).
C_L	cLitter	Litter carbon pool size (calibration target).
C_S	cSoil	Soil carbon pool size (calibration target).
N_P	nVeg	Vegetation nitrogen pool size (i.e., plant nitrogen pool size) (calibration target).
N_L	nLitter	Litter nitrogen pool size (calibration target).
N_S	nSoil	Soil nitrogen pool size (calibration target).
N_M	nMineral	Mineral nitrogen pool size (calibration target).
AD	fNdep	Nitrogen deposition on land (model input).
FT	fNfert	Nitrogen fertilizer application (model input).
NPP2X	–	X = P (plant), L (litter), or S (soil); Fraction of NPP that goes into plant, litter, or soil pool within the 1-year time step.
PU2X	–	X = P (plant), L (litter), or S (soil); Fraction of PU that goes into plant, litter, or soil pool within the 1-year time step.
BNF2X	–	X = P (plant), L (litter), or S (soil); Fraction of BNF that goes into plant, litter, or soil pool within the 1-year time step.
cLP (or nLP)	–	Carbon (or nitrogen) flux from litter production (i.e., leaf dropping).
cLP2X (or nLP2X)	–	X = L (litter) or S (soil); Fraction of cLP (or nLP) that goes into litter or soil pool within the 1-year time step.
cLD (or nLD)	–	Carbon (or nitrogen) flux from litter decomposition. Within 1-year timescale, it includes the litter decomposition to soil organic matters, and the subsequent mineralization of fresh/labile soil organic matters (fast).
cLD2X (or nLD2X)	–	X = S (soil), A (atmosphere) or M (mineral); Fraction of cLD that goes into soil and atmosphere pool (or nLD that goes into soil and mineral pool) within the 1-year time step.
cSR (or nSR)	–	Carbon (or nitrogen) flux from soil respiration. It is mainly from decomposition of recalcitrant soil organic matter (slow) when a litter pool is present.
nLS	–	Nitrogen flux from the mineral nitrogen loss.
nLSgas, nLSleach	–	nLS in terms of gaseous loss or leaching loss.
cLUnet, cLUgrs, cLUrgr (or nLUnet, nLUgrs, nLUrgr)	–	Carbon (or nitrogen) flux from land use perturbation in terms of net emission, gross deforestation, and regrowth, respectively.
$cLUgrs_X$ (or $nLUgrs_X$)	–	X = P (plant), L (litter), or S (soil); Fraction of cLUgrs (or nLUgrs) that occurs in plant, litter, or soil pool.
nLUmin	–	Direct mineral nitrogen loss from land use perturbation.
C_{Land} (or N_{Land})	cLand (or nLand)	Total land carbon (or nitrogen) pool size; C_{Land} is the sum of C_P, C_L, and C_S. N_{Land} is the sum of N_P, N_L, N_S, and N_M.
N_{Lando}	–	Total land organic nitrogen pool size; N_{Land} is the sum of N_P, N_L, and N_S.
cNetLand (or nNetLand)	nbp (for carbon)	Net land carbon (or nitrogen) flux from land to atmosphere (i.e., net biosphere production for carbon).

Conflict of Interest

The authors declare no conflicts of interest relevant to this study.

Data Availability Statement

The CNit v2.0 model code and the calibrated parameters for the studied CMIP6 Earth system models are available at https://doi.org/10.5281/zenodo.15569386 (Tang, Zaehle, et al., 2025). The accompanying Python code is primarily intended to support review and reproducibility and includes essential documentation. A ready-to-use, standalone Python package for CNit is now available on PyPI (https://pypi.org/project/cnit), with full documentation hosted at https://cnit.readthedocs.io. The source code is publicly available on GitHub (https://github.com/gangtang-au/cnit). The MAGICC Fortran code, including the MAGICC-CNit implementation, is available on GitLab at https://gitlab.com/magicc/magicc.

Calibration data are available from the Earth System Grid Federation (ESGF, https://esgf-node.llnl.gov/projects/cmip6/) for original CMIP6 ESM outputs, and from https://doi.org/10.5281/zenodo.14060168 (Tang et al., 2024) for the processed global annual-mean data. See Section 3.1, "Target Variables, Experiments, and CMIP6 ESMs," and Section 3.2, "Data Collection and Post-Processing," for details.

Acknowledgments

Gang Tang acknowledges support from the Guest Program at the Max Planck Institute for Biogeochemistry (MPI-BGC), as well as the Science Abroad Travelling Scholarships and the School of Geography, Earth and Atmospheric Sciences Graduate Researcher Travelling Funds from The University of Melbourne. Sönke Zaehle and Zebedee Nicholls acknowledge funding from the European Union's Horizon 2020 research and innovation programme (ESM2025, Grant 101003536). Tilo Ziehn and Malte Meinshausen acknowledge support from the National Environmental Science Program (Climate Systems Hub), funded by the Australian Government Department of Climate Change, Energy, the Environment, and Water. The authors thank Chris Jones from the Met Office Hadley Centre for his valuable comments on an earlier draft. We also express our sincere gratitude to the World Climate Research Programme (WCRP), the Coupled Model Intercomparison Project Phase 6 (CMIP6), the Earth system model (ESM) groups, the Coupled Climate–Carbon Cycle Model Intercomparison Project (C4MIP) and related MIPs, and the Earth System Grid Federation (ESGF) for their invaluable collaborative efforts in making ESM outputs openly available and accessible. The authors thank the three anonymous reviewers for their very positive feedback and constructive comments and suggestions, which helped improve the clarity of the manuscript.

Author Contributions: GT and MM conceptualized the initial idea of incorporating carbon-nitrogen coupling in MAGICC. GT designed, implemented, and calibrated both CNit v1.0 and v2.0. SZ, ZN, AN, and MM contributed to model development, with SZ providing key suggestions and valuable input on parameterizing the carbon-nitrogen coupling effect on net primary production–one of the major updates in CNit v2.0. ZN supported code development and optimization for both model versions, as well as calibration implementation. SZ, AN, and TZ contributed to the interpretation and in-depth discussion of the results. SZ, ZN, TZ, and MM were responsible for funding acquisition, and MM, SZ, ZN, and AN supervised the project. GT conducted the analysis, interpreted the results, and wrote the first draft of the manuscript. All authors contributed to reviewing and revising the manuscript. Open Access funding enabled and organized by Projekt DEAL.

References

Aerts, R., & Chapin, F. S. (1999). The mineral nutrition of wild plants revisited: A re-evaluation of processes and patterns. In A. H. Fitter & D. G. Raffaelli (Eds.), *Advances in Ecological Research* (pp. 1–67). Academic Press. https://doi.org/10.1016/S0065-2504(08)60016-1

Anav, A., Friedlingstein, P., Kidston, M., Bopp, L., Ciais, P., Cox, P., et al. (2013). Evaluating the land and ocean components of the global carbon cycle in the CMIP5 Earth System Models. *Journal of Climate*, *26*(18), 6801–6843. https://doi.org/10.1175/JCLI-D-12-00417.1

Arora, V. K., Katavouta, A., Williams, R. G., Jones, C. D., Brovkin, V., Friedlingstein, P., et al. (2020). Carbon–concentration and carbon–climate feedbacks in CMIP6 models and their comparison to CMIP5 models. *Biogeosciences*, *17*(16), 4173–4222. https://doi.org/10.5194/bg-17-4173-2020

Boucher, O., Servonnat, J., Albright, A. L., Aumont, O., Balkanski, Y., Bastrikov, V., et al. (2020). Presentation and evaluation of the IPSL-CM6A-LR climate model. *Journal of Advances in Modeling Earth Systems*, *12*(7), e2019MS002010. https://doi.org/10.1029/2019MS002010

Byers, E., Krey, V., Kriegler, E., Riahi, K., Schaeffer, R., Kikstra, J., et al. (2022). AR6 scenarios database [Dataset]. *Zenodo*. https://doi.org/10.5281/zenodo.5886911

Cheng, Y., Wang, J., Chang, S. X., Cai, Z., Müller, C., & Zhang, J. (2019). Nitrogen deposition affects both net and gross soil nitrogen transformations in forest ecosystems: A review. *Environmental Pollution*, *244*, 608–616. https://doi.org/10.1016/j.envpol.2018.10.054

Danabasoglu, G., Lamarque, J. F., Bacmeister, J., Bailey, D. A., DuVivier, A. K., Edwards, J., et al. (2020). The Community Earth System Model Version 2 (CESM2). *Journal of Advances in Modeling Earth Systems*, *12*, e2019MS001916. https://doi.org/10.1029/2019MS001916

Davies-Barnard, T., & Friedlingstein, P. (2020). The global distribution of biological nitrogen fixation in terrestrial natural ecosystems. *Global Biogeochemical Cycles*, *34*(3), e2019GB006387. https://doi.org/10.1029/2019GB006387

Davies-Barnard, T., Meyerholt, J., Zaehle, S., Friedlingstein, P., Brovkin, V., Fan, Y., et al. (2020). Nitrogen cycling in CMIP6 land surface models: Progress and limitations. *Biogeosciences*, *17*(20), 5129–5148. https://doi.org/10.5194/bg-17-5129-2020

Davies-Barnard, T., Zaehle, S., & Friedlingstein, P. (2022). Assessment of the impacts of biological nitrogen fixation structural uncertainty in CMIP6 earth system models. *Biogeosciences*, *19*(14), 3491–3503. https://doi.org/10.5194/bg-19-3491-2022

Du, Z., Weng, E., Jiang, L., Luo, Y., Xia, J., & Zhou, X. (2018). Carbon–nitrogen coupling under three schemes of model representation: A traceability analysis. *Geoscientific Model Development*, *11*, 4399–4416. https://doi.org/10.5194/gmd-11-4399-2018

Eberwein, J. R., Oikawa, P. Y., Allsman, L. A., & Jenerette, G. D. (2015). Carbon availability regulates soil respiration response to nitrogen and temperature. *Soil Biology and Biochemistry*, *88*, 158–164. https://doi.org/10.1016/j.soilbio.2015.05.014

Feng, M., Peng, S., Wang, Y., Ciais, P., Goll, D. S., Chang, J., et al. (2023). Overestimated nitrogen loss from denitrification for natural terrestrial ecosystems in CMIP6 Earth System Models. *Nature Communications*, *14*(1), 3065. https://doi.org/10.1038/s41467-023-38803-z

Fleischer, K., Dolman, A. J., van der Molen, M. K., Rebel, K. T., Erisman, J. W., Wassen, M. J., et al. (2019). Nitrogen deposition maintains a positive effect on terrestrial carbon sequestration in the 21st century despite growing phosphorus limitation at regional scales. *Global Biogeochemical Cycles*, *33*(6), 810–824. https://doi.org/10.1029/2018GB005952

Gao, F., & Han, L. (2012). Implementing the Nelder-Mead simplex algorithm with adaptive parameters. *Computational Optimization and Applications*, *51*(1), 259–277. https://doi.org/10.1007/s10589-010-9329-3

Gidden, M. J., Riahi, K., Smith, S. J., Fujimori, S., Luderer, G., Kriegler, E., et al. (2019). Global emissions pathways under different socioeconomic scenarios for use in CMIP6: A dataset of harmonized emissions trajectories through the end of the century. *Geoscientific Model Development*, *12*(4), 1443–1475. https://doi.org/10.5194/gmd-12-1443-2019

Gier, B. K., Schlund, M., Friedlingstein, P., Jones, C. D., Jones, C., Zaehle, S., & Eyring, V. (2024). Representation of the terrestrial carbon cycle in CMIP6. *Biogeosciences*, *21*(22), 5321–5360. https://doi.org/10.5194/bg-21-5321-2024

Goll, D. S., Winkler, A. J., Raddatz, T., Dong, N., Prentice, I. C., Ciais, P., & Brovkin, V. (2017). Carbon–nitrogen interactions in idealized simulations with JSBACH (version 3.10). *Geoscientific Model Development*, *10*(5), 2009–2030. https://doi.org/10.5194/gmd-10-2009-2017

Gütschow, J., Jeffery, M. L., Gieseke, R., Gebel, R., Stevens, D., Krapp, M., & Rocha, M. (2016). The PRIMAP-hist national historical emissions time series. *Earth System Science Data*, *8*(2), 571–603. https://doi.org/10.5194/essd-8-571-2016

Hajima, T., Watanabe, M., Yamamoto, A., Tatebe, H., Noguchi, M. A., Abe, M., et al. (2020). Development of the MIROC-ES2L Earth system model and the evaluation of biogeochemical processes and feedbacks. *Geoscientific Model Development*, *13*(5), 2197–2244. https://doi.org/10.5194/gmd-13-2197-2020

He, L., Chen, J. M., Croft, H., Gonsamo, A., Luo, X., Liu, J., et al. (2017). Nitrogen availability dampens the positive impacts of CO_2 fertilization on terrestrial ecosystem carbon and water cycles. *Geophysical Research Letters*, *44*(22), 11590–11600. https://doi.org/10.1002/2017GL075981

Hegglin, M., Kinnison, D., & Lamarque, J.-F. (2016). CCMI nitrogen surface fluxes in support of CMIP6—Version 2.0 [Dataset]. *Earth System Grid Federation*. https://doi.org/10.22033/esgf/input4mips.1125

Hu, Q., Li, T., Deng, X., Wu, T., Zhai, P., Huang, D., et al. (2022). Intercomparison of global terrestrial carbon fluxes estimated by MODIS and Earth system models. *Science of the Total Environment*, *810*, 152231. https://doi.org/10.1016/j.scitotenv.2021.152231

Hungate, B. A., Dukes, J. S., Shaw, M. R., Luo, Y., & Field, C. B. (2003). Nitrogen and climate change. *Science*, *302*(5650), 1512–1513. https://doi.org/10.1126/science.1091390

Huntingford, C., Burke, E. J., Jones, C. D., Jeffers, E. S., & Wiltshire, A. J. (2022). Nitrogen cycle impacts on CO_2 fertilisation and climate forcing of land carbon stores. *Environmental Research Letters*, *17*(4), 044072. https://doi.org/10.1088/1748-9326/ac6148

Hurtt, G. C., Chini, L., Sahajpal, R., Frolking, S., Bodirsky, B. L., Calvin, K., et al. (2020). Harmonization of global land use change and management for the period 850–2100 (LUH2) for CMIP6. *Geoscientific Model Development*, *13*(11), 5425–5464. https://doi.org/10.5194/gmd-13-5425-2020

Janssens, I. A., Dieleman, W., Luyssaert, S., Subke, J. A., Reichstein, M., Ceulemans, R., et al. (2010). Reduction of forest soil respiration in response to nitrogen deposition. *Nature Geoscience*, *3*(5), 315–322. https://doi.org/10.1038/ngeo844

Jiang, M., Medlyn, B. E., Drake, J. E., Duursma, R. A., Anderson, I. C., Barton, C. V. M., et al. (2020). The fate of carbon in a mature forest under carbon dioxide enrichment. *Nature*, *580*(7802), 227–231. https://doi.org/10.1038/s41586-020-2128-9

Knorr, M., Frey, S. D., & Curtis, P. S. (2005). Nitrogen additions and litter decomposition: A meta-analysis. *Ecology*, *86*(12), 3252–3257. https://doi.org/10.1890/05-0150

Kolby Smith, W., Reed, S. C., Cleveland, C. C., Ballantyne, A. P., Anderegg, W. R. L., Wieder, W. R., et al. (2016). Large divergence of satellite and Earth system model estimates of global terrestrial CO_2 fertilization. *Nature Climate Change*, *6*(3), 306–310. https://doi.org/10.1038/nclimate2879

Kou-Giesbrecht, S., Arora, V. K., Jones, C. D., Brovkin, V., Hajima, T., Kawamiya, M., et al. (2025). Rising nitrogen deposition leads to only a minor increase in CO_2 uptake in Earth system models. *Communications Earth & Environment*, *6*(1), 216. https://doi.org/10.1038/s43247-024-01943-1

Kou-Giesbrecht, S., Arora, V. K., Seiler, C., Arneth, A., Falk, S., Jain, A. K., et al. (2023). Evaluating nitrogen cycling in terrestrial biosphere models: A disconnect between the carbon and nitrogen cycles. *Earth System Dynamics*, *14*(4), 767–795. https://doi.org/10.5194/esd-14-767-2023

Krishna, M. P., & Mohan, M. (2017). Litter decomposition in forest ecosystems: A review. *Energy, Ecology and Environment*, *2*(4), 236–249. https://doi.org/10.1007/s40974-017-0064-9

Le Quéré, C., Andrew, R. M., Canadell, J. G., Sitch, S., Korsbakken, J. I., Peters, G. P., et al. (2016). Global Carbon Budget 2016. *Earth System Science Data*, *8*(2), 605–649. https://doi.org/10.5194/essd-8-605-2016

Li, F., Guo, D., Gao, X., & Zhao, X. (2021). Water deficit modulates the CO_2 fertilization effect on plant gas exchange and leaf-level water use efficiency: A meta-analysis. *Frontiers in Plant Science*, *12*, 775477. https://doi.org/10.3389/fpls.2021.775477

Liu, H., Mi, Z., Lin, L., Wang, Y., Zhang, Z., Zhang, F., et al. (2018). Shifting plant species composition in response to climate change stabilizes grassland primary production. *Proceedings of the National Academy of Sciences of the United States of America*, *115*(16), 4051–4056. https://doi.org/10.1073/pnas.1700299114

Lovato, T., Peano, D., Butenschön, M., Materia, S., Iovino, D., Scoccimarro, E., et al. (2022). CMIP6 Simulations with the CMCC Earth System Model (CMCC-ESM2). *Journal of Advances in Modeling Earth Systems*, *14*(3), e2021MS002814. https://doi.org/10.1029/2021MS002814

Maag, M., & Vinther, F. P. (1996). Nitrous oxide emission by nitrification and denitrification in different soil types and at different soil moisture contents and temperatures. *Applied Soil Ecology*, *4*(1), 5–14. https://doi.org/10.1016/0929-1393(96)00106-0

Mauritsen, T., Bader, J., Becker, T., Behrens, J., Bittner, M., Brokopf, R., et al. (2019). Developments in the MPI-M Earth System Model version 1.2 (MPI-ESM1.2) and its response to increasing CO_2. *Journal of Advances in Modeling Earth Systems*, *11*(4), 998–1038. https://doi.org/10.1029/2018MS001400

McClaugherty, C. A., Pastor, J., Aber, J. D., & Melillo, J. M. (1985). Forest litter decomposition in relation to soil nitrogen dynamics and litter quality. *Ecology*, *66*(1), 266–275. https://doi.org/10.2307/1941327

McGrath, J. M., & Lobell, D. B. (2013). Regional disparities in the CO_2 fertilization effect and implications for crop yields. *Environmental Research Letters*, *8*(1), 014054. https://doi.org/10.1088/1748-9326/8/1/014054

McNeill, A., & Unkovich, M. (2007). The nitrogen cycle in terrestrial ecosystems. In P. Marschner & Z. Rengel (Eds.), *Nutrient Cycling in Terrestrial Ecosystems* (pp. 37–64). Springer Berlin Heidelberg. https://doi.org/10.1007/978-3-540-68027-7_2

Meinshausen, M., Nicholls, Z. R. J., Lewis, J., Gidden, M. J., Vogel, E., Freund, M., et al. (2020). The shared socio-economic pathway (SSP) greenhouse gas concentrations and their extensions to 2500. *Geoscientific Model Development*, *13*(8), 3571–3605. https://doi.org/10.5194/gmd-13-3571-2020

Meinshausen, M., Raper, S. C. B., & Wigley, T. M. L. (2011). Emulating coupled atmosphere-ocean and carbon cycle models with a simpler model, MAGICC6—Part 1: Model description and calibration. *Atmospheric Chemistry and Physics*, *11*(4), 1417–1456. https://doi.org/10.5194/acp-11-1417-2011

Meinshausen, M., Vogel, E., Nauels, A., Lorbacher, K., Meinshausen, N., Etheridge, D. M., et al. (2017). Historical greenhouse gas concentrations for climate modelling (CMIP6). *Geoscientific Model Development*, *10*(5), 2057–2116. https://doi.org/10.5194/gmd-10-2057-2017

Meyerholt, J., Sickel, K., & Zaehle, S. (2020). Ensemble projections elucidate effects of uncertainty in terrestrial nitrogen limitation on future carbon uptake. *Global Change Biology*, *26*(7), 3978–3996. https://doi.org/10.1111/gcb.15114

Meyerholt, J., Zaehle, S., & Smith, M. J. (2016). Variability of projected terrestrial biosphere responses to elevated levels of atmospheric CO_2 due to uncertainty in biological nitrogen fixation. *Biogeosciences*, *13*(5), 1491–1518. https://doi.org/10.5194/bg-13-1491-2016

Nicholls, Z., Meinshausen, M., Lewis, J., Corradi, M. R., Dorheim, K., Gasser, T., et al. (2021). Reduced complexity model intercomparison project phase 2: Synthesizing Earth system knowledge for probabilistic climate projections. *Earth's Future*, *9*(6), e2020EF001900. https://doi.org/10.1029/2020EF001900

O'Neill, B. C., Tebaldi, C., van Vuuren, D. P., Eyring, V., Friedlingstein, P., Hurtt, G., et al. (2016). The Scenario Model Intercomparison Project (ScenarioMIP) for CMIP6. *Geoscientific Model Development*, *9*, 3461–3482. https://doi.org/10.5194/gmd-9-3461-2016

Pornon, A., Marty, C., Winterton, P., & Lamaze, T. (2011). The intriguing paradox of leaf lifespan responses to nitrogen availability. *Functional Ecology*, *25*(4), 796–801. https://doi.org/10.1111/j.1365-2435.2011.01849.x

Rabin, S. S., Melton, J. R., Lasslop, G., Bachelet, D., Forrest, M., Hantson, S., et al. (2017). The Fire Modeling Intercomparison Project (FireMIP), phase 1: Experimental and analytical protocols with detailed model descriptions. *Geoscientific Model Development*, *10*(3), 1175–1197. https://doi.org/10.5194/gmd-10-1175-2017

Reich, P. B., Walters, M. B., & Ellsworth, D. S. (1997). From tropics to tundra: Global convergence in plant functioning. *Proceedings of the National Academy of Sciences of the United States of America*, *94*(25), 13730–13734. https://doi.org/10.1073/pnas.94.25.13730

Schimel, D., Stephens, B. B., & Fisher, J. B. (2015). Effect of increasing CO_2 on the terrestrial carbon cycle. *Proceedings of the National Academy of Sciences of the United States of America*, *112*(2), 436–441. https://doi.org/10.1073/pnas.1407302112

Séférian, R., Nabat, P., Michou, M., Saint-Martin, D., Voldoire, A., Colin, J., et al. (2019). Evaluation of CNRM Earth System Model, CNRM-ESM2-1: Role of Earth system processes in present-day and future climate. *Journal of Advances in Modeling Earth Systems*, *11*(12), 4182–4227. https://doi.org/10.1029/2019MS001791

Seiler, C., Kou-Giesbrecht, S., Arora, V. K., & Melton, J. R. (2024). The impact of climate forcing biases and the nitrogen cycle on land carbon balance projections. *Journal of Advances in Modeling Earth Systems*, *16*(1), e2023MS003749. https://doi.org/10.1029/2023MS003749

Seland, Ø., Bentsen, M., Olivié, D., Toniazzo, T., Gjermundsen, A., Graff, L. S., et al. (2020). Overview of the Norwegian Earth System Model (NorESM2) and key climate response of CMIP6 DECK, historical, and scenario simulations. *Geoscientific Model Development*, *13*(12), 6165–6200. https://doi.org/10.5194/gmd-13-6165-2020

Sellar, A. A., Walton, J., Jones, C. G., Wood, R., Abraham, N. L., Andrejczuk, M., et al. (2020). Earth System models for CMIP6. *Journal of Advances in Modeling Earth Systems*, *12*(4), e2019MS001946. https://doi.org/10.1029/2019MS001946

Sigmond, M., Anstey, J., Arora, V., Digby, R., Gillett, N., Kharin, V., et al. (2023). Improvements in the Canadian Earth System Model (CanESM) through systematic model analysis: CanESM5.0 and CanESM5.1. *Geoscientific Model Development*, *16*(22), 6553–6591. https://doi.org/10.5194/gmd-16-6553-2023

Sokolov, A. P., Kicklighter, D. W., Melillo, J. M., Felzer, B. S., Schlosser, C. A., & Cronin, T. W. (2008). Consequences of considering carbon–nitrogen interactions on the feedbacks between climate and the terrestrial carbon cycle. *Journal of Climate*, *21*(15), 3776–3796. https://doi.org/10.1175/2008JCLI2038.1

Storn, R., & Price, K. (1997). Differential evolution—A simple and efficient heuristic for global optimization over continuous spaces. *Journal of Global Optimization*, *11*(4), 341–359. https://doi.org/10.1023/A:1008202821328

Sun, Z., Liu, L., Ma, Y., Yin, G., Zhao, C., Zhang, Y., & Piao, S. (2014). The effect of nitrogen addition on soil respiration from a nitrogen-limited forest soil. *Agricultural and Forest Meteorology*, *197*, 103–110. https://doi.org/10.1016/j.agrformet.2014.06.010

Tang, G., Nicholls, Z., Jones, C., Gasser, T., Norton, A., Ziehn, T., et al. (2024). Code and data for "investigating carbon and nitrogen conservation in reported CMIP6 Earth System Model Data" [Dataset]. *Zenodo*. https://doi.org/10.5281/zenodo.14060168

Tang, G., Nicholls, Z., Jones, C., Gasser, T., Norton, A., Ziehn, T., et al. (2025). Investigating carbon and nitrogen conservation in reported CMIP6 Earth system model data. *Geoscientific Model Development*, *18*(7), 2111–2136. https://doi.org/10.5194/gmd-18-2111-2025

Tang, G., Nicholls, Z., Norton, A., Zaehle, S., & Meinshausen, M. (2025). Synthesizing global carbon–nitrogen coupling effects—The MAGICC coupled carbon–nitrogen cycle model v1.0. *Geoscientific Model Development*, *18*(7), 2193–2230. https://doi.org/10.5194/gmd-18-2193-2025

Tang, G., Zaehle, S., Nicholls, Z., Norton, A., Ziehn, T., & Meinshausen, M. (2025). Model source code for the MAGICC coupled carbon–nitrogen cycle model—CNit. https://doi.org/10.5281/zenodo.15569386

Thornton, P. E., Lamarque, J.-F., Rosenbloom, N. A., & Mahowald, N. M. (2007). Influence of carbon-nitrogen cycle coupling on land model response to CO_2 fertilization and climate variability. *Global Biogeochemical Cycles*, *21*(4). https://doi.org/10.1029/2006GB002868

Tietjen, B., Schlaepfer, D. R., Bradford, J. B., Lauenroth, W. K., Hall, S. A., Duniway, M. C., et al. (2017). Climate change-induced vegetation shifts lead to more ecological droughts despite projected rainfall increases in many global temperate drylands. *Global Change Biology*, *23*(7), 2743–2754. https://doi.org/10.1111/gcb.13598

Trenberth, K. E. (2011). Changes in precipitation with climate change. *Climate Research*, *47*(1), 123–138. https://doi.org/10.3354/cr00953

Varney, R. M., Chadburn, S. E., Burke, E. J., & Cox, P. M. (2022). Evaluation of soil carbon simulation in CMIP6 Earth system models. *Biogeosciences*, *19*, 4671–4704. https://doi.org/10.5194/bg-19-4671-2022

Varney, R. M., Friedlingstein, P., Chadburn, S. E., Burke, E. J., & Cox, P. M. (2024). Soil carbon-concentration and carbon-climate feedbacks in CMIP6 Earth system models. *Biogeosciences*, *21*(11), 2759–2776. https://doi.org/10.5194/bg-21-2759-2024

Vitousek, P. M., Menge, D. N., Reed, S. C., & Cleveland, C. C. (2013). Biological nitrogen fixation: Rates, patterns and ecological controls in terrestrial ecosystems. *Philosophical Transactions of the Royal Society B: Biological Sciences*, *368*(1621), 20130119. https://doi.org/10.1098/rstb.2013.0119

Walker, A. P., De Kauwe, M. G., Medlyn, B. E., Zaehle, S., Iversen, C. M., Asao, S., et al. (2019). Decadal biomass increment in early secondary succession woody ecosystems is increased by CO_2 enrichment. *Nature Communications*, *10*(1), 454. https://doi.org/10.1038/s41467-019-08348-1

Wang, S., Zhang, Y., Ju, W., Chen, J. M., Ciais, P., Cescatti, A., et al. (2020). Recent global decline of CO_2 fertilization effects on vegetation photosynthesis. *Science*, *370*(6522), 1295–1300. https://doi.org/10.1126/science.abb7772

Wang, Y.-C., Hsu, H.-H., Chen, C.-A., Tseng, W.-L., Hsu, P.-C., Lin, C.-W., et al. (2021). Performance of the Taiwan Earth system model in simulating climate variability compared with observations and CMIP6 model simulations. *Journal of Advances in Modeling Earth Systems*, *13*(7), e2020MS002353. https://doi.org/10.1029/2020MS002353

Wei, N., Xia, J., Zhou, J., Jiang, L., Cui, E., Ping, J., & Luo, Y. (2022). Evolution of uncertainty in terrestrial carbon storage in Earth system models from CMIP5 to CMIP6. *Journal of Climate*, *35*(17), 5483–5499. https://doi.org/10.1175/JCLI-D-21-0763.1

Wigley, T. M. L., & Raper, S. C. B. (1987). Thermal expansion of sea water associated with global warming. *Nature*, *330*(6144), 127–131. https://doi.org/10.1038/330127a0

Wigley, T. M. L., & Raper, S. C. B. (1992). Implications for climate and sea level of revised IPCC emissions scenarios. *Nature*, *357*(6376), 293–300. https://doi.org/10.1038/357293a0

Wigley, T. M. L., & Raper, S. C. B. (2001). Interpretation of high projections for global-mean warming. *Science*, *293*(5529), 451–454. https://doi.org/10.1126/science.1061604

Wu, T., Yu, R., Lu, Y., Jie, W., Fang, Y., Zhang, J., et al. (2021). BCC-CSM2-HR: A high-resolution version of the Beijing Climate Center Climate System Model. *Geoscientific Model Development*, *14*(5), 2977–3006. https://doi.org/10.5194/gmd-14-2977-2021

Zaehle, S., Friend, A. D., Friedlingstein, P., Dentener, F., Peylin, P., & Schulz, M. (2010). Carbon and nitrogen cycle dynamics in the O-CN land surface model: 2. Role of the nitrogen cycle in the historical terrestrial carbon balance. *Global Biogeochemical Cycles*, *24*(1). https://doi.org/10.1029/2009GB003522

Zaehle, S., Jones, C. D., Houlton, B., Lamarque, J.-F., & Robertson, E. (2015). Nitrogen availability reduces CMIP5 projections of twenty-first-century land carbon uptake. *Journal of Climate*, *28*(6), 2494–2511. https://doi.org/10.1175/JCLI-D-13-00776.1

Zaehle, S., Medlyn, B. E., De Kauwe, M. G., Walker, A. P., Dietze, M. C., Hickler, T., et al. (2014). Evaluation of 11 terrestrial carbon–nitrogen cycle models against observations from two temperate Free-Air CO2 Enrichment studies. *New Phytologist*, *202*(3), 803–822. https://doi.org/10.1111/nph.12697

Zeng, W., Wang, Z., Chen, X., Yao, X., Ma, Z., & Wang, W. (2023). Nitrogen deficiency accelerates soil organic carbon decomposition in temperate degraded grasslands. *Science of the Total Environment*, *881*, 163424. https://doi.org/10.1016/j.scitotenv.2023.163424

Zhang, X., Zhang, Y., Tian, J., Ma, N., & Wang, Y.-P. (2022). CO_2 fertilization is spatially distinct from stomatal conductance reduction in controlling ecosystem water-use efficiency increase. *Environmental Research Letters*, *17*(5), 054048. https://doi.org/10.1088/1748-9326/ac6c9c

Zhu, J., Gao, X., & Zeng, X. (2022). Response of terrestrial net primary production to climate change associated with the quadrupling CO_2 forcing in CMIP6 models. *Atmospheric Science Letters*, *23*(9), e1098. https://doi.org/10.1002/asl.1098

Ziehn, T., Chamberlain, M. A., Law, R. M., Lenton, A., Bodman, R. W., Dix, M., et al. (2020). The Australian Earth System model: ACCESS-ESM1.5. *Journal of Southern Hemisphere Earth Systems Science*, *70*(1), 193–214. https://doi.org/10.1071/ES19035

Ziehn, T., Wang, Y. P., & Huang, Y. (2021). Land carbon-concentration and carbon-climate feedbacks are significantly reduced by nitrogen and phosphorus limitation. *Environmental Research Letters*, *16*(7), 074043. https://doi.org/10.1088/1748-9326/ac0e62

Zohner, C. M., Mirzagholi, L., Renner, S. S., Mo, L., Rebindaine, D., Bucher, R., et al. (2023). Effect of climate warming on the timing of autumn leaf senescence reverses after the summer solstice. *Science*, *381*(6653), eadf5098. https://doi.org/10.1126/science.adf5098